JEM Journal of Experimental Medicine

ARTICLE

PD-1 restraint of regulatory T cell suppressive activity is critical for immune tolerance

Catherine L. Tan[1,2*], Juhi R. Kuchroo[1,2*], Peter T. Sage[1,2], Dan Liang[1,2], Loise M. Francisco[1,2], Jessica Buck[1,2], Youg Raj Thaker[1,2,3], Qianxia Zhang[4,5], Shannon L. McArdel[1,2], Vikram R. Juneja[1,2], Sun Jung Lee[1,2], Scott B. Lovitch[1,6], Christine Lian[6], George F. Murphy[6], Bruce R. Blazar[7], Dario A.A. Vignali[4,5,8], Gordon J. Freeman[9,10], and Arlene H. Sharpe[1,2,6]

Inhibitory signals through the PD-1 pathway regulate T cell activation, T cell tolerance, and T cell exhaustion. Studies of PD-1 function have focused primarily on effector T cells. Far less is known about PD-1 function in regulatory T (T reg) cells. To study the role of PD-1 in T reg cells, we generated mice that selectively lack PD-1 in T reg cells. PD-1–deficient T reg cells exhibit an activated phenotype and enhanced immunosuppressive function. The in vivo significance of the potent suppressive capacity of PD-1–deficient T reg cells is illustrated by ameliorated experimental autoimmune encephalomyelitis (EAE) and protection from diabetes in nonobese diabetic (NOD) mice lacking PD-1 selectively in T reg cells. We identified reduced signaling through the PI3K–AKT pathway as a mechanism underlying the enhanced suppressive capacity of PD-1–deficient T reg cells. Our findings demonstrate that cell-intrinsic PD-1 restraint of T reg cells is a significant mechanism by which PD-1 inhibitory signals regulate T cell tolerance and autoimmunity.

Introduction

The programmed death (PD)–1 pathway delivers inhibitory signals that control the magnitude of adaptive immune responses and tolerance (Bour-Jordan et al., 2011; Pauken and Wherry, 2015; Sharpe and Pauken, 2018). The PD-1 receptor is inducibly expressed on conventional $CD4^+$ and $CD8^+$ T cells as well as $CD4^+FOXP3^+$ T regulatory (T reg) cells during immune activation and chronic inflammation (Flies et al., 2011; Okazaki et al., 2013; Riley, 2009). PD-1 inhibitory signals play critical roles in regulating the threshold for T cell activation and limiting effector T (Teff) cell responses, as well as controlling T cell tolerance, resolution of inflammation, and T cell exhaustion. The two PD-1 ligands, PD-L1 (B7-H1, CD274) and PD-L2 (B7-DC, CD273), are expressed on hematopoietic cells (Liang et al., 2003; Schreiner et al., 2004), nonhematopoietic cells (Keir et al., 2006; Scandiuzzi et al., 2014), and tumor cells (Juneja et al., 2017; Patel and Kurzrock, 2015; Yearley et al., 2017). Their expression in tissue can dampen T cell responses locally to limit tissue injury and maintain tissue tolerance (Barber et al., 2006; Keir et al., 2006; Reynoso et al., 2009; Scandiuzzi et al., 2014).

The PD-1 pathway has proven an attractive target for cancer immunotherapy. PD-1 or PD-L1 blockade is approved by the US Food and Drug Administration for the treatment of >20 types of cancer, including melanoma, non–small cell lung cancer, renal cell carcinoma, Hodgkin's lymphoma, and DNA mismatch repair–deficient adult and pediatric solid tumors (Callahan et al., 2016; Sharpe and Pauken, 2018). Given these clinical successes and the increasing use of PD-1 blockade therapeutically, a better understanding of how disruption of this pathway influences immune responses is needed.

The functions of PD-1 inhibitory signals are best understood in effector $CD4^+$ and $CD8^+$ T cells. It is not yet clear how PD-1 impacts T reg cell activation and effector functions. Previous studies have demonstrated that PD-1 signals are important for induced T reg (iT reg) cell development (Amarnath et al., 2011; Francisco et al., 2009; Wang et al., 2008), but the in vivo role of PD-1 in other types of T reg cells remains poorly understood. T reg cells critically control immune responses by restraining immune effector cells (Hori et al., 2003; Fontenot et al., 2003; Vignali et al., 2008; Josefowicz et al., 2012; Smigiel et al., 2014).

[1]Department of Immunology, Blavatnik Institute, Harvard Medical School, Boston, MA; [2]Evergrande Center for Immunological Diseases, Harvard Medical School and Brigham and Women's Hospital, Boston, MA; [3]School of Life Sciences, University of Essex, Wivenhoe Park, Colchester, UK; [4]Department of Immunology, University of Pittsburgh School of Medicine, Pittsburgh, PA; [5]Tumor Microenvironment Center, UPMC Hillman Cancer Center, Pittsburgh, PA; [6]Department of Pathology, Brigham and Women's Hospital and Harvard Medical School, Boston, MA; [7]Department of Pediatrics, University of Minnesota Medical School, Twin Cities, MN; [8]Cancer Immunology and Immunotherapy Program, UPMC Hillman Cancer Center, Pittsburgh PA; [9]Department of Medical Oncology, Dana-Farber Cancer Institute, Boston, MA; [10]Harvard Medical School, Boston, MA.

*C.L. Tan and J.R. Kuchroo contributed equally to this paper; Correspondence to Arlene H. Sharpe: arlene_sharpe@hms.harvard.edu.

Beyond ensuring immune homeostasis, T reg cells play significant roles in many diseases, including autoimmunity, transplant rejection, infections, and cancer, making them attractive targets for therapeutic intervention (Chapman and Chi, 2014; Bluestone et al., 2015; Rosenblum et al., 2012). However, in order to modulate T reg cells effectively, the signals that control T reg cell activity need to be better understood.

In this study, we use T reg cell–specific PD-1 conditional knockout strategies to investigate the role of PD-1 signals in controlling T reg cell activation and function. We demonstrate that PD-1 inhibits T reg cell activation and suppressive capacity. The in vivo significance of the potent suppressive capacity of PD-1–deficient T reg cells is illustrated by ameliorated experimental autoimmune encephalomyelitis (EAE) and protection from diabetes in nonobese diabetic (NOD) mice lacking PD-1 selectively in T reg cells. Our findings establish PD-1 restraint of T reg cells as a new mechanism by which PD-1 inhibitory signals regulate T cell tolerance and autoimmunity.

Results

PD-1–deficient T reg cells exhibit an activated phenotype

To determine how PD-1 controls T reg cells, we generated PD-1 floxed mice (*Pdcd1*$^{fl/fl}$; Fig. S1 A) and crossed them to *Foxp3*^{Cre} mice (Rubtsov et al., 2008) to generate mice in which PD-1 could be selectively deleted in T reg cells, referred to as *Foxp3*^{Cre} *Pdcd1*$^{fl/fl}$ mice (Fig. S1 B). We assessed efficiency of PD-1 deletion on T reg cells in thymus, lung, inguinal LNs, and spleen in these mice at 4–5 wk of age and 8 wk of age (Fig. S1, C and D). At both ages, we observed near-complete loss of PD-1 on T reg cells in all organs assessed. We then characterized the T reg cell compartment in the *Foxp3*^{Cre} *Pdcd1*$^{fl/fl}$ mice. The expression level of FOXP3 (Fig. 1 A) was similar in PD-1–deficient and WT T reg cells. There was a small increase in the frequency of T reg cells in the spleen of *Foxp3*^{Cre} *Pdcd1*$^{fl/fl}$ mice compared with *Foxp3*^{Cre} *Pdcd1*$^{wt/wt}$ littermates (~19% versus ~17%; Fig. 1 B) and a higher frequency of activated T reg cells at baseline, based on CD44^{hi} CD62L^{lo} expression (~56% versus ~38%; Fig. 1 C). We also observed higher Ki67 expression in *Foxp3*^{Cre} *Pdcd1*$^{fl/fl}$ mice compared with WT T reg cells (~48% versus ~38%; Fig. 1 D) at baseline. In addition, a higher percentage of PD-1–deficient T reg cells expressed CTLA-4 (Fig. 1 E), ICOS (Fig. 1 F), TIGIT (Fig. 1 G), and GITR (Fig. 1 H). Since both CTLA-4 and TIGIT expression levels have been correlated with increased T reg cell suppressive capacity (Joller et al., 2014), these findings suggest that PD-1–deficient T reg cells may be more potent suppressors than WT T reg cells.

PD-1–deficient T reg cells are more immunosuppressive than WT T reg cells in vitro

To determine how PD-1 deficiency affects T reg cell functions, we first used an in vitro T reg cell suppression assay. T reg cells were isolated from *Foxp3*^{Cre} *Pdcd1*$^{fl/fl}$ or control *Foxp3*^{Cre} *Pdcd1*$^{fl/wt}$ mice and cultured with naive WT CD4$^+$ FOXP3$^-$ Teff cells in the presence of irradiated APCs and stimulated with anti-CD3 for 3–4 d. *Foxp3*^{Cre} *Pdcd1*$^{fl/fl}$ T reg cells suppressed proliferation of CD4$^+$ FOXP3$^-$ Teff cells (Fig. 2, A–C) more effectively than littermate control *Foxp3*^{Cre} *Pdcd1*$^{fl/wt}$ T reg cells. In addition, IL-17A (Fig. 2 D) and TNF-α production (Fig. 2 E) was more reduced in cultures with *Foxp3*^{Cre} *Pdcd1*$^{fl/fl}$ T reg cells. Thus, loss of PD-1 in T reg cells increases their capacity to inhibit CD4$^+$FOXP3$^-$ Teff cell proliferation and cytokine production in vitro. These findings indicate that PD-1 can restrain T reg cell suppressive function in vitro.

Since studies have demonstrated that PD-1 signals are important for the generation of iT reg cells (Amarnath et al., 2011; Francisco et al., 2009; Wang et al., 2008), we also assessed if PD-1 deletion in T reg cells affected the generation of iT reg cells from naive CD4$^+$ T cells isolated from *Foxp3*^{Cre} *Pdcd1*$^{fl/fl}$ mice. We compared the generation of iT reg cells from naive CD4$^+$ T cells isolated from *Foxp3*^{Cre} *Pdcd1*$^{fl/fl}$ mice and *Foxp3*^{Cre} *Pdcd1*$^{wt/wt}$ control mice (Fig. S2 A) and found a slight reduction in frequencies of iT reg cells generated from *Foxp3*^{Cre} *Pdcd1*$^{fl/fl}$ mice (Fig. S2 B). These PD-1–deficient iT reg cells also exhibited a slightly lower FOXP3 mean fluorescence intensity (Fig. S2 C). Overall, these findings suggest that *Foxp3*^{Cre} *Pdcd1*$^{fl/fl}$ mice have no overt defect in iT reg cell generation.

Inducible deletion of PD-1 in T reg cells ameliorates EAE

To determine how PD-1 controls T reg cell functions in vivo, we crossed *Pdcd1*$^{fl/fl}$ mice to *Foxp3*$^{ERT2.Cre}$ mice (referred to as *iFoxp3*^{Cre} *Pdcd1*$^{fl/fl}$ mice) to generate mice in which PD-1 could be inducibly and selectively deleted in T reg cells following tamoxifen administration. We examined the effects of deleting PD-1 on T reg cells in an induced mouse model of autoimmunity, EAE, because previous studies using PD-1– and PD-L1–deficient mice or PD-1 pathway–blocking antibodies have demonstrated the importance of the PD-1 pathway in attenuating EAE (Kroner et al., 2009; Salama et al., 2003; Wang et al., 2009; Latchman et al., 2004). We first assessed efficiency of deletion of PD-1 in the spleen and central nervous system (CNS) by administering 5 (Fig. S1 E) or 10 (Fig. S1 F) doses of tamoxifen to *iFoxp3*^{Cre} *Pdcd1*$^{fl/fl}$ and *iFoxp3*^{Cre} *Pdcd1*$^{wt/wt}$ and then inducing EAE with MOG_{35-55}/CFA. We evaluated deletion at day 12–13 after immunization. We found that the greatest proportion of PD-1 loss occurred after the first five doses of tamoxifen but maximal deletion was achieved after 10 doses. Based on our findings, we administered 10 doses of tamoxifen to achieve maximal deletion of PD-1. We then immunized *iFoxp3*^{Cre} *Pdcd1*$^{fl/fl}$ and *iFoxp3*^{Cre} *Pdcd1*$^{wt/wt}$ with MOG_{35-55}/CFA to induce EAE. *iFoxp3*^{Cre} *Pdcd1*$^{fl/fl}$ mice developed less severe EAE compared with littermate *iFoxp3*^{Cre} *Pdcd1*$^{wt/wt}$ control mice (Fig. 3 A). There was efficient deletion of PD-1 in T reg cells in the CNS of *iFoxp3*^{Cre} *Pdcd1*$^{fl/fl}$ mice (Fig. 3 B). PD-1–deleted mice had a small but significant increase in the frequency of FoxP3$^+$ T reg cells compared with littermate control mice (Fig. 3 C) but similar T reg cell numbers at the peak of disease (Fig. 3 D). In addition, there were reduced frequencies of IFN-γ– and IL-17A–producing CD4$^+$ FOXP3$^-$ Teff cells in the CNS and cervical LNs of *iFoxp3*^{Cre} *Pdcd1*$^{fl/fl}$ compared with *iFoxp3*^{Cre} *Pdcd1*$^{wt/wt}$ mice (Fig. 3, E and F). The attenuated EAE severity upon inducible PD-1 deletion in T reg cells likely reflects increased T reg cell proportions in the CNS and enhanced T reg cell–mediated suppression of Teff cell proinflammatory cytokine production.

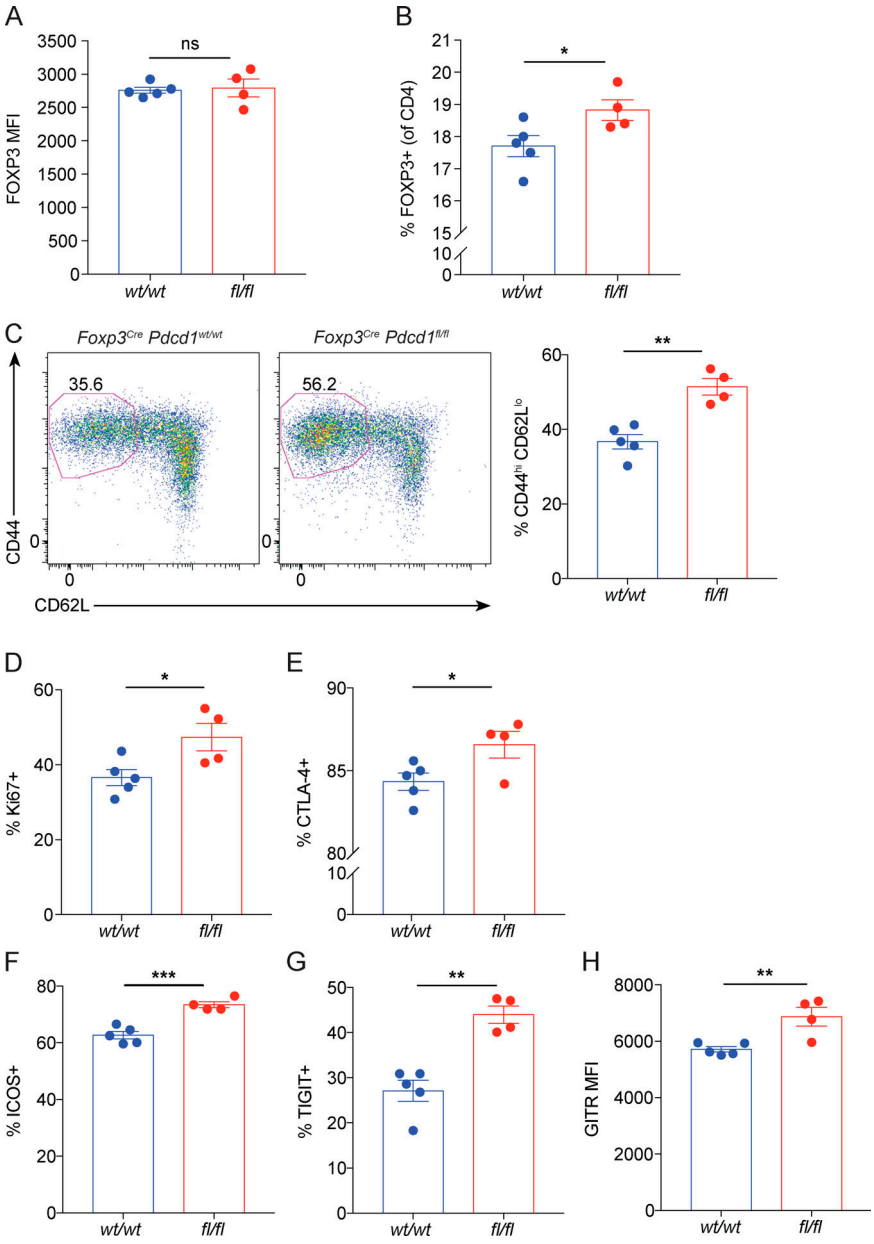

Figure 1. **PD-1–deficient T reg cells exhibit an activated phenotype. (A and B)** Age-matched *Foxp3*^{Cre} *Pdcd1*$^{wt/wt}$ (*wt/wt*, blue, *n* = 5) and *Foxp3*^{Cre} *Pdcd1*$^{fl/fl}$ (*fl/fl*, red, *n* = 4) littermates were analyzed for FOXP3 mean fluorescence intensity (MFI; A) and frequency of T reg cells of total CD4$^+$ T cells in the spleen (B). **(C)** Representative flow cytometry plot (left) and percentages (right) of CD44^{hi}CD62L^{lo} T reg cells in spleen of *Foxp3*^{Cre} *Pdcd1*$^{wt/wt}$ (*wt/wt*, blue), and *Foxp3*^{Cre} *Pdcd1*$^{fl/fl}$ (*fl/fl*, red) littermates. **(D–G)** Percentages of T reg cells expressing (D) Ki67, (E) CTLA-4, (F) ICOS, and (G) TIGIT were compared in *Foxp3*^{Cre} *Pdcd1*$^{wt/wt}$ (*wt/wt*, blue, *n* = 5) and *Foxp3*^{Cre} *Pdcd1*$^{fl/fl}$ (*fl/fl*, red, *n* = 4) mice. **(H)** GITR expression level was assessed in T reg cells from *Foxp3*^{Cre} *Pdcd1*$^{wt/wt}$ (*wt/wt*, blue, *n* = 5) and *Foxp3*^{Cre} *Pdcd1*$^{fl/fl}$ (*fl/fl*, red, *n* = 4) littermates. Significance was assessed using unpaired Student's *t* test (A–H). Data are representative of three independent experiments. Data are shown as means ± SEM. *, P < 0.05; **, P < 0.01; ***, P < 0.005. ns, not significant.

To understand if the altered function of PD-1–deficient T reg cells is due to a cell-intrinsic change, we undertook studies to compare PD-1–expressing (PD-1$^+$) and nonexpressing (PD-1$^-$) T reg cells within the same microenvironment. To do so, we administered a suboptimal dose of tamoxifen (5 doses of tamoxifen instead of 10) to *iFoxp3*^{Cre} *Pdcd1*$^{fl/fl}$ mice such that a population of PD-1–expressing T reg cells was still present and subsequently induced EAE in these mice. This experimental setup allowed us to compare PD-1–deficient and expressing T reg cells in the same microenvironment. We analyzed T reg cells in the spleen and CNS at the peak of EAE. We first gated on CD44$^+$ T reg cells to capture T reg cells that were activated and, for this reason, would have up-regulated PD-1 in response to activating signals (Fig. 3 G). Only after gating on CD44$^+$ T reg cells did we then gate on PD-1$^+$ and PD-1$^-$ populations. This strategy allowed us to select for T reg cells that lost PD-1 in response to tamoxifen administration rather than those that were PD-1 low because they had never been activated and had never up-regulated the PD-1 receptor. Using this strategy, we found that PD-1$^-$ T reg cells expressed a higher frequency of Ki67 compared with PD-1$^+$ T reg cells in the same microenvironment (Fig. 3 H). These findings demonstrate that PD-1 controls expansion of T reg cells in a cell-intrinsic manner. Thus, loss of PD-1 on T reg cells leads to an increased frequency of FOXP3$^+$ T reg cells compared with FOXP3$^-$ Teff cells.

NOD mice that selectively lack PD-1 in T reg cells are protected from type 1 diabetes

To further dissect the role of PD-1 in T reg cells in tolerance and autoimmunity, we evaluated PD-1 function in T reg cells in a mouse model of spontaneous autoimmunity, the NOD mouse model of type 1 diabetes. The PD-1–PD-L1 pathway limits the

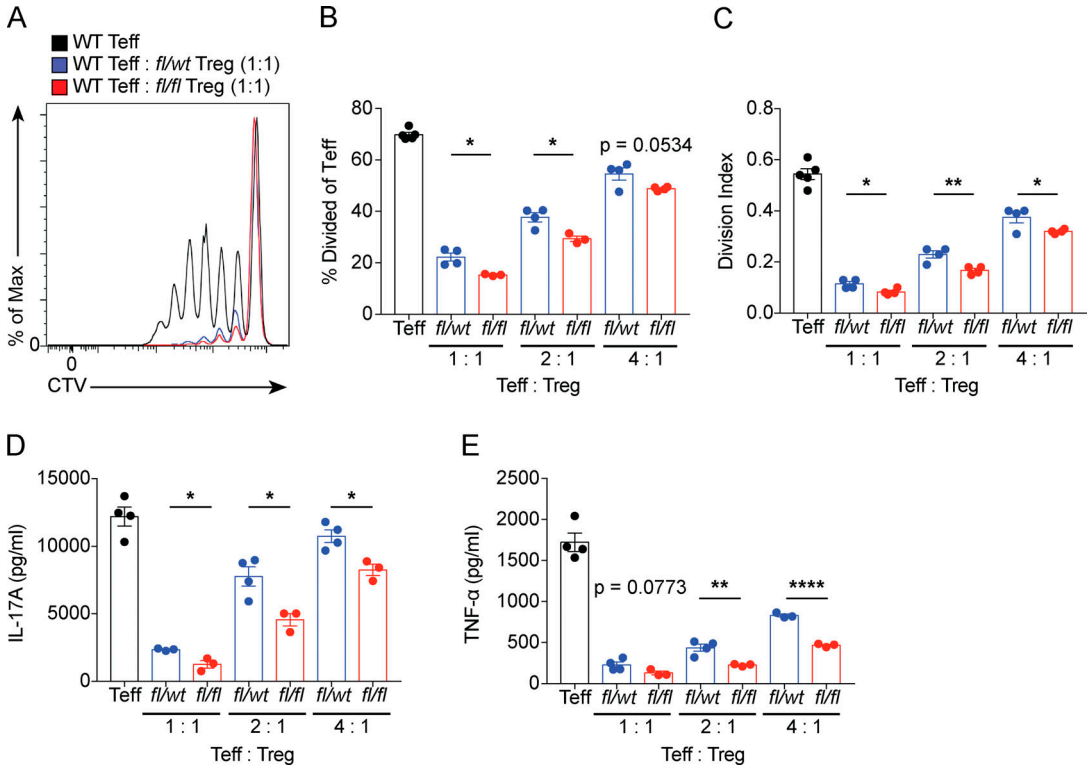

Figure 2. **PD-1–deficient T reg cells have enhanced suppressive capacity.** In vitro T reg cell–mediated suppression assay in which *Foxp3*^{Cre} *Pdcd1*$^{wt/fl}$ (blue, *n* = 4) and *Foxp3*^{Cre} *Pdcd1*$^{fl/fl}$ (*fl/fl*, red, *n* = 3) T reg cells were sorted from littermate mice and cultured with CD4$^+$ FoxP3$^-$ Teff cells and irradiated APCs and activated with 1 µg/ml anti-CD3 at 1:1, 2:1, and 4:1 Teff to T reg cell ratios. **(A)** After 3–4 d of culture, Teff cell proliferation was measured by CTV dilution. **(B–E)** Quantification of Teff cell proliferation (B and C). Culture supernatants were analyzed for IL-17A (D) and (E) TNF-α at day 3 of culture from assays as in A. Significance was assessed using unpaired Student's *t* test (B–E). Data are representative of at least three independent experiments. Data are represented means ± SEM. *, P < 0.05; **, P < 0.01; ****, P < 0.001.

initiation and progression of diabetes in NOD mice (Wang et al., 2005, Ansari et al., 2003, Paterson et al., 2011, Keir et al., 2006). We crossed the *Pdcd1*$^{fl/fl}$ mice onto the NOD background and bred them with *NOD.Foxp3*^{Cre} mice (Zhou et al., 2008) to generate *NOD.Foxp3*$^{Cre+}$ *Pdcd1*$^{fl/fl}$ mice. NOD females lacking PD-1 specifically in T reg cells were protected from diabetes in two different animal facilities: 0% versus ∼50% incidence in controls in an animal facility at Harvard (Fig. 4 A) and 0% versus ∼60% incidence in controls in an animal facility at the University of Pittsburgh (Fig. S3 A). In the Harvard mouse facility, control littermates began to develop diabetes at 14 wk of age, whereas none of the 19 *NOD.Foxp3*$^{Cre+}$ *Pdcd1*$^{fl/fl}$ mice developed hyperglycemia by 40 wk of age. These findings indicate that PD-1 curbs T reg cell function during NOD diabetes. The protection of NOD mice from diabetes in two different animal facilities suggests that environmental influences cannot explain the protective effects of PD-1 deficiency in T reg cells.

Certain hallmarks of diabetes pathology in NOD mice are well known, including development of peri-insulitis in prediabetic animals and progression to insulitis, characterized by leukocyte infiltration and islet destruction. Histopathologic comparison of pancreata from mice at 14 wk of age, a time point before diabetes onset, revealed that *NOD.Foxp3*$^{Cre+}$ *Pdcd1*$^{fl/fl}$ mice had significantly fewer islets with peri-insulitis compared with *NOD.Foxp3*$^{Cre-}$ *Pdcd1*$^{fl/fl}$ littermate controls, reflecting attenuated disease development (Fig. 4 B and Fig. S3 B).

To determine the cellular mechanism by which *NOD.Foxp3*$^{Cre+}$ *Pdcd1*$^{fl/fl}$ mice are protected from diabetes, we compared T reg, CD4$^+$ FOXP3$^-$ T and CD8$^+$ Teff cells in the pancreas, pancreatic LNs (pLNs), and nondraining inguinal LNs (ndLNs) of 14-wk-old nondiabetic *NOD.Foxp3*$^{Cre+}$ *Pdcd1*$^{fl/fl}$ and *NOD.Foxp3*$^{Cre-}$ *Pdcd1*$^{fl/fl}$ littermate controls. The frequencies of T reg cells relative to CD4$^+$ FoxP3$^-$ (Fig. 4 C) and CD8$^+$ Teff cells (Fig. 4 D) were significantly altered (higher in the pancreas but lower in the pLNs and ndLNs of the *NOD.Foxp3*^{Cre} *Pdcd1*$^{fl/fl}$ mice as compared with controls). Moreover, there were significantly reduced numbers of CD4$^+$ FOXP3$^-$ Teff cells (Fig. S3 C) and CD8$^+$ Teff cells (Fig. S3 D), but comparable numbers of T reg cells (Fig. S3 E) in the pancreas of *NOD.Foxp3*$^{Cre+}$ *Pdcd1*$^{fl/fl}$ compared with littermate controls. In addition, expansion of CD4$^+$ FOXP3$^-$ and CD8$^+$ Teff cells was suppressed significantly by *NOD.Foxp3*$^{Cre+}$ *Pdcd1*$^{fl/fl}$ T reg cells compared with *NOD.Foxp3*$^{Cre-}$ *Pdcd1*$^{fl/fl}$ T reg cells, as indicated by decreased Ki67 expression in CD4$^+$ FOXP3$^-$ effector (Fig. S3 F) and CD8$^+$ T cells (Fig. 4 E) from the pancreata of *NOD.Foxp3*$^{Cre+}$ *Pdcd1*$^{fl/fl}$ mice. Furthermore, the frequencies of pancreatic CD4$^+$ FOXP3$^-$ (Fig. S3 G) and CD8$^+$ (Fig. 4 F) Teff cells producing IFN-γ or coproducing IFN-γ and TNF-α were reduced in *NOD.Foxp3*$^{Cre+}$ *Pdcd1*$^{fl/fl}$ mice compared with littermate controls. Collectively, these data demonstrate that *NOD.Foxp3*$^{Cre+}$ *Pdcd1*$^{fl/fl}$ T reg cells

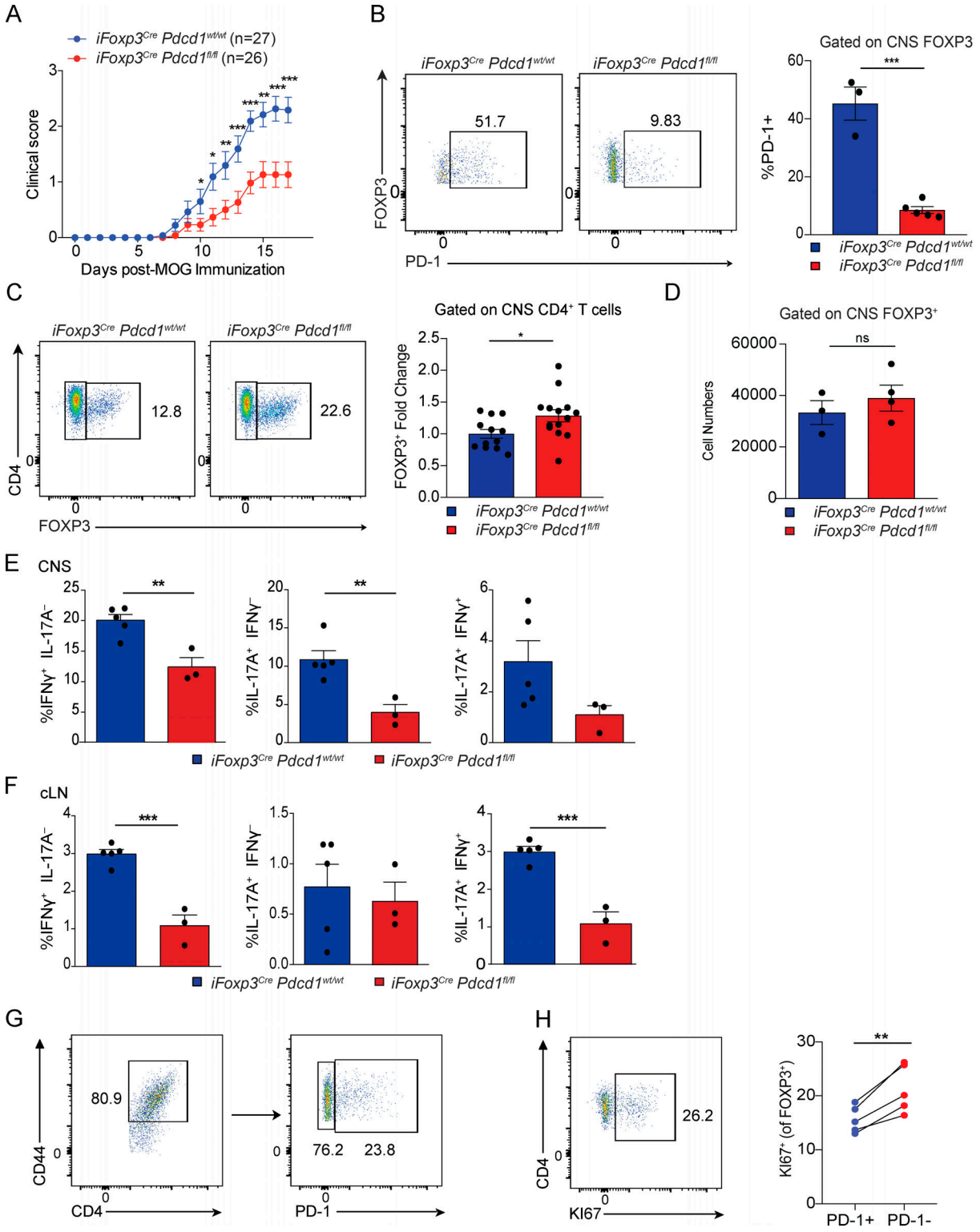

Figure 3. **Inducible deletion of PD-1 in T reg cells results in protection from EAE. (A)** *iFoxp3*^{Cre} *Pdcd1*$^{wt/wt}$ (blue circles, *n* = 27) or *iFoxp3*^{Cre} *Pdcd1*$^{fl/fl}$ (red circles, *n* = 26) mice were given tamoxifen for 10 d and then immunized with MOG_{35-55}/CFA 5 d after the last tamoxifen dose to induce EAE. Mice were monitored daily for signs of clinical disease. **(B)** Representative flow cytometry plots (left panel) and comparison of PD-1 expression in T reg cells from the CNS of *iFoxp3*^{Cre} *Pdcd1*$^{wt/wt}$ (*n* = 3) and *iFoxp3*^{Cre} *Pdcd1*$^{fl/fl}$ (*n* = 5) mice at peak of disease (right panel). **(C–F)** Representative flow cytometry plots (left panel) with frequency of FOXP3$^+$ T reg cells of CD4$^+$ T cells expressed as a fold change of PD-1–deficient (*n* = 14) versus control mice (*n* = 12; C) and numbers of T reg cells of total CD4$^+$ from the CNS of *iFoxp3*^{Cre} *Pdcd1*$^{wt/wt}$ (*n* = 3) and *iFoxp3*^{Cre} *Pdcd1*$^{fl/fl}$ (*n* = 5) mice following immunization (D). CD4$^+$ FOXP3$^-$ Teff cells were analyzed for IFN-γ and IL-17A production in the CNS (E) or cervical LN ([cLN]; F) by intracellular staining from *iFoxp3*^{Cre} *Pdcd1*$^{wt/wt}$ (*n* = 5) and *iFoxp3*^{Cre} *Pdcd1*$^{fl/fl}$ (*n* = 3) mice. **(G and H)** *iFoxp3*^{Cre} *Pdcd1*$^{fl/fl}$ mice (*n* = 5) were given five doses of tamoxifen to achieve a suboptimal deletion of PD-1 and subsequently immunized with MOG_{35-55}/CFA and analyzed at peak of disease. **(G)** Representative gating schematic to analyze PD-1–deleted and expressing T reg cells from the spleen after

pregating on CD44$^+$ FOXP3$^+$ cells. **(H)** Representative flow cytometry plot (left panel) and Ki67 expression (right panel) on PD-1–deficient and PD-1–expressing T reg cells from the spleen after pregating as described in G. Data in B–D and G–H are from littermates. Data are pooled from four independent experiments (A), representative of three independent experiments (B, E, and F), from two pooled experiments (C), or representative of two independent experiments (D, G, and H). A Mann–Whitney nonparametric test was used (A and C), and significance was assessed using an unpaired Student's *t* test (B and D–F) or paired Student's *t* test (H). Data are represented means ± SEM. *, P < 0.05; **, P < 0.01; ***, P < 0.005. ns, not significant.

suppress the activation, expansion, and effector functions of diabetogenic Teff cells more potently than control *NOD.Foxp3^{Cre}-Pdcd1$^{fl/fl}$* T reg cells.

PD-1–deficient BDC2.5 T reg cells have a competitive advantage over WT BDC2.5 T reg cells

Cell-extrinsic factors such as the inflammatory cytokine milieu could potentially contribute to differences between T reg cells seen in the WT and PD-1–deficient NOD strains. To directly assess whether PD-1–deficient NOD T reg cells have a cell-intrinsic advantage over WT NOD T reg cells in the same tissue microenvironment receiving the same antigen and cytokine cues, we used an adoptive transfer approach. We crossed BDC2.5 TCR (chromogranin A–specific) transgenic mice with *NOD.Foxp3^{Cre} Pdcd1$^{fl/fl}$* mice and then cotransferred an equal number of congenically marked *NOD.Foxp3^{Cre+} Pdcd1$^{fl/wt}$ BDC2.5$^+$ Thy$^{1.1/1.2}$* T reg cells and *NOD.Foxp3^{Cre+} Pdcd1$^{fl/fl}$ BDC2.5$^+$ Thy$^{1.2/1.2}$* T reg cells into *NOD Thy$^{1.1/1.1}$* recipients (Fig. 5 A) and compared their functions. At 4 d after adoptive transfer, we examined the cotransferred T reg cells in the nondraining LNs, pLNs, and pancreas by first gating on CD4$^+$ Vβ4$^+$ Thy$^{1.2+}$ using flow cytometry followed by subsetting by Thy1.1 to differentiate between PD-1–deficient *NOD.Foxp3^{Cre+}Pdcd1$^{fl/fl}$ BDC2.5$^+$ Thy$^{1.2/1.2}$* T reg and control *NOD.FoxP3^{Cre+} Pdcd1$^{fl/wt}$ BDC2.5$^+$ Thy$^{1.1/1.2}$* T reg cells. PD-1–deficient *NOD.Foxp3^{Cre+} Pdcd1$^{fl/fl}$ BDC2.5$^+$ Thy$^{1.2/1.2}$* T reg cells significantly outcompeted control *NOD.Foxp3^{Cre+} Pdcd1$^{fl/wt}$ BDC2.5$^+$ Thy$^{1.1/1.2}$* T reg cells in the pancreas (∼68% versus ∼31%) and pLNs (∼57% versus ∼42%; Fig. 5, B and C).

We assessed whether this competitive advantage was due to increased proliferation by labeling *NOD.Foxp3^{Cre+} Pdcd1$^{fl/fl}$ BDC2.5$^+$ Thy$^{1.2}$* T reg cells and *NOD.Foxp3^{Cre+} Pdcd1$^{fl/wt}$ BDC2.5$^+$ Thy$^{1.1/1.2}$* T reg cells with a proliferation dye and cotransferring them at equal ratios into *NOD Thy$^{1.1}$* recipients. PD-1–deficient *NOD.Foxp3^{Cre+} Pdcd1$^{fl/fl}$ BDC2.5$^+$ Thy$^{1.2}$* T reg cells had a modest increase in proliferation compared with control *NOD.Foxp3^{Cre+} Pdcd1$^{fl/wt}$ BDC2.5$^+$ Thy$^{1.1/1.2}$* T reg cells in the pLN, but not in the pancreas (Fig. 5 D). Thus, similarly to EAE, these studies further demonstrate that PD-1 can control expansion of T reg cells in a cell-intrinsic manner.

PD-1–deficient T reg cells exhibit alterations in PI3K–AKT pathway

To determine mechanisms by which PD-1 controls T reg cell functions, we used a transcriptomic approach. We induced EAE in *Foxp3^{GFP}* and *Foxp3$^{Cre.YFP/wt}$ PD-1$^{fl/fl}$* mice, sorted GFP- or YFP-expressing T reg cells from the CNS at the peak of disease when mice had a similar clinical disease score, and performed bulk RNA sequencing (RNA-seq) to compare the transcriptional profiles of WT and PD-1–deficient T reg cells (Fig. 6 A and Fig. S4 A). Transcriptomic analysis revealed differences in a number of genes (Fig. 6 B and Fig. S4, B and C) and pathways (Table S1) between WT and PD-1–deficient T reg cells. Gene set enrichment analyses revealed down-regulation of genes in the PI3K–AKT–mTOR signaling pathway in PD-1–deficient T reg cells compared with WT T reg cells (Fig. 6 C). Notably, the PI3K–AKT–mTOR signaling pathway has been implicated in control of T reg cell function (Sauer et al., 2008; Haxhinasto et al., 2008; Chapman and Chi, 2014).

We validated the findings from transcriptional profiling using phospho-flow cytometry. Consistent with the gene set enrichment analysis, PD-1–deficient T reg cells have reduced pAKT (Fig. 6 D) and pS6 (Fig. 6 E) compared with WT T reg cells, suggesting that *Foxp3^{Cre} Pdcd1$^{fl/fl}$* T reg cells have reduced signaling through the PI3K–AKT pathway. In addition, there were reduced levels of pFOXO1/3A (Fig. S4 D) and CCR7 (Fig. S4 E), both downstream targets of the PI3K–AKT pathway. PTEN levels were reduced in *Foxp3^{Cre} Pdcd1$^{fl/fl}$* T reg cells compared with WT T reg cells (Fig. S4 F), suggesting that down-regulation of the PI3K–AKT pathway may be independent of PTEN in PD-1–deficient T reg cells. Our finding that PD-1–deficient T reg cells have reduced PI3K–AKT signaling suggests that the enhanced suppressive function of PD-1–deficient T reg cells may be due to down-regulation of the PI3K–AKT pathway, because previous studies have shown activation of AKT results in reduced T reg cell suppressive capacity (Crellin et al., 2007; Gerriets et al., 2016).

PD-1–deficient T reg cells have altered bioenergetics

There is growing recognition that changes in metabolism are vital for optimal cellular differentiation and effector functions (MacIver et al., 2013; Buck et al., 2015). Previous studies have suggested a role for PD-1 inhibitory signals in reducing signaling through the PI3K–AKT pathway (Parry et al., 2005; Patsoukis et al., 2013; Riley, 2009; Francisco et al., 2009; Patsoukis et al., 2012) and altering cell metabolism in Teff cells (Patsoukis et al., 2015). How PD-1–mediated signaling regulates metabolism in T reg cells, however, remains unclear. The alterations in the PI3K–AKT pathway in PD-1–deficient T reg cells led us to investigate whether PD-1–deficient T reg cells have altered cellular bioenergetics. We first compared the glycolytic capabilities of WT and PD-1–deficient T reg cells using a glycolysis stress test. For these studies, we sort-purified WT and PD-1–deficient T reg cells from the spleens of unmanipulated *Foxp3^{GFP}* mice and *Pdcd1$^{-/-}$ Foxp3^{GFP}* mice using CD4$^+$ FOXP3.GFP$^+$ and stimulated the T reg cells in vitro with plate-bound anti-CD3, anti-CD28, and 500 U/ml IL-2 for 16 h. The next day we replated the T reg cells and used an extracellular flux analyzer to measure the extracellular acidification rate (ECAR). ECAR is an indicator of glycolysis because as cells undergo glycolysis, protons are produced and extruded, causing acidification of the surroundings.

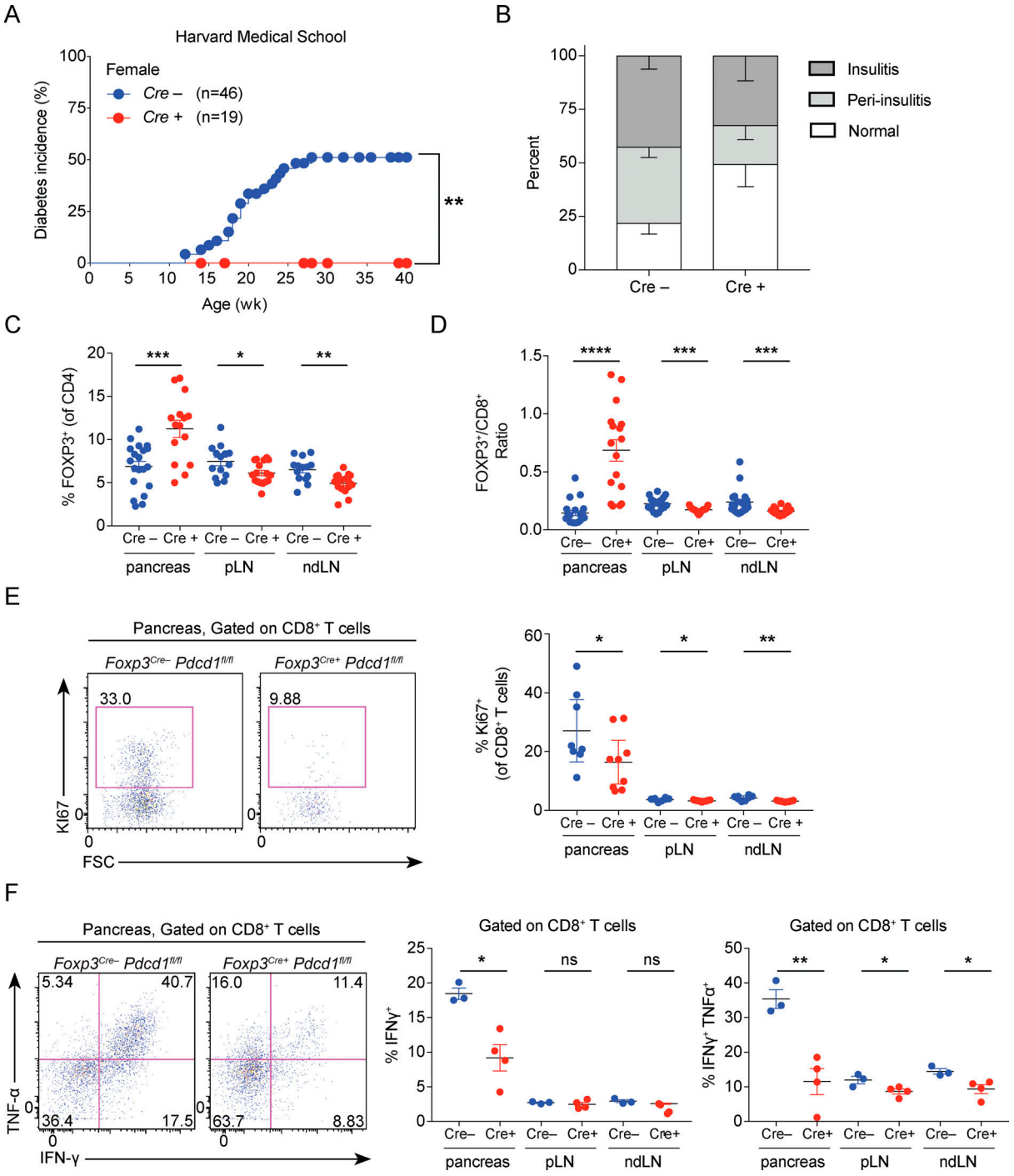

Figure 4. **NOD mice lacking PD-1 selectively in T reg cells are protected from type 1 diabetes. (A)** Diabetes onset and incidence were monitored in female *NOD.Foxp3^{Cre+} Pdcd1$^{fl/fl}$* (red, *n* = 19) and *NOD.Foxp3^{Cre-} Pdcd1$^{fl/fl}$* (blue, *n* = 46) littermates in an animal facility at Harvard Medical School to up to 40 wk of age. **(B)** Insulitis scores from *NOD.Foxp3^{Cre+} Pdcd1$^{fl/fl}$* (*n* = 11) and *NOD.Foxp3^{Cre-} Pdcd1$^{fl/fl}$* (*n* = 13) littermate controls at 14 wk of age. **(C and D)** Percentages of CD4$^+$ FOXP3$^+$ T reg cells of total CD4$^+$ T cells (C) and ratio of CD4$^+$ FOXP3$^+$ T reg cells relative to CD8$^+$ T cells (D) in the pancreas, pLNs, and inguinal LNs (ndLN) from *Foxp3^{Cre+} Pdcd1$^{fl/fl}$* (Cre+, red circles, *n* = 17) and *Foxp3^{Cre-} Pdcd1$^{fl/fl}$* (Cre–, blue circles, *n* = 20) littermate controls at 14 wk of age. **(E)** Representative flow cytometry plots (left panel) and percentages (right panel) of Ki67-expressing CD8β$^+$ T cells from the pancreas, pLN, and ndLN of prediabetic *NOD.Foxp3^{Cre-} Pdcd1$^{fl/fl}$* (Cre–, blue circles, *n* = 8) and *NOD.Foxp3^{Cre+} Pdcd1$^{fl/fl}$* (Cre+, red circles, *n* = 9) mice at 14 wk of age. **(F)** CD8$^+$ T cells from the pancreas, pLN, and ndLN of prediabetic *NOD.Foxp3^{Cre-} Pdcd1$^{fl/fl}$* (Cre–, blue circles, *n* = 3) and *NOD.Foxp3^{Cre+} Pdcd1$^{fl/fl}$* (Cre+, red circles, *n* = 4) mice were analyzed for IFN-γ and TNF-α production by intracellular staining at 14 wk of age. Representative flow cytometry plots (left panel) and percentages (right panel) of IFN-γ and TNF-α production from pancreatic CD8$^+$ T cells are shown. Data are pooled from four independent experiments (C and D) or representative of two independent experiments (E and F). A log-rank (Mantel–Cox) test (A), Mann–Whitney nonparametric test (C and D), or Student's *t* test (E and F) was used. Data are shown as means ± SEM. *, P < 0.05; **, P < 0.01; ***, P < 0.005; ****, P < 0.001. ns, not significant.

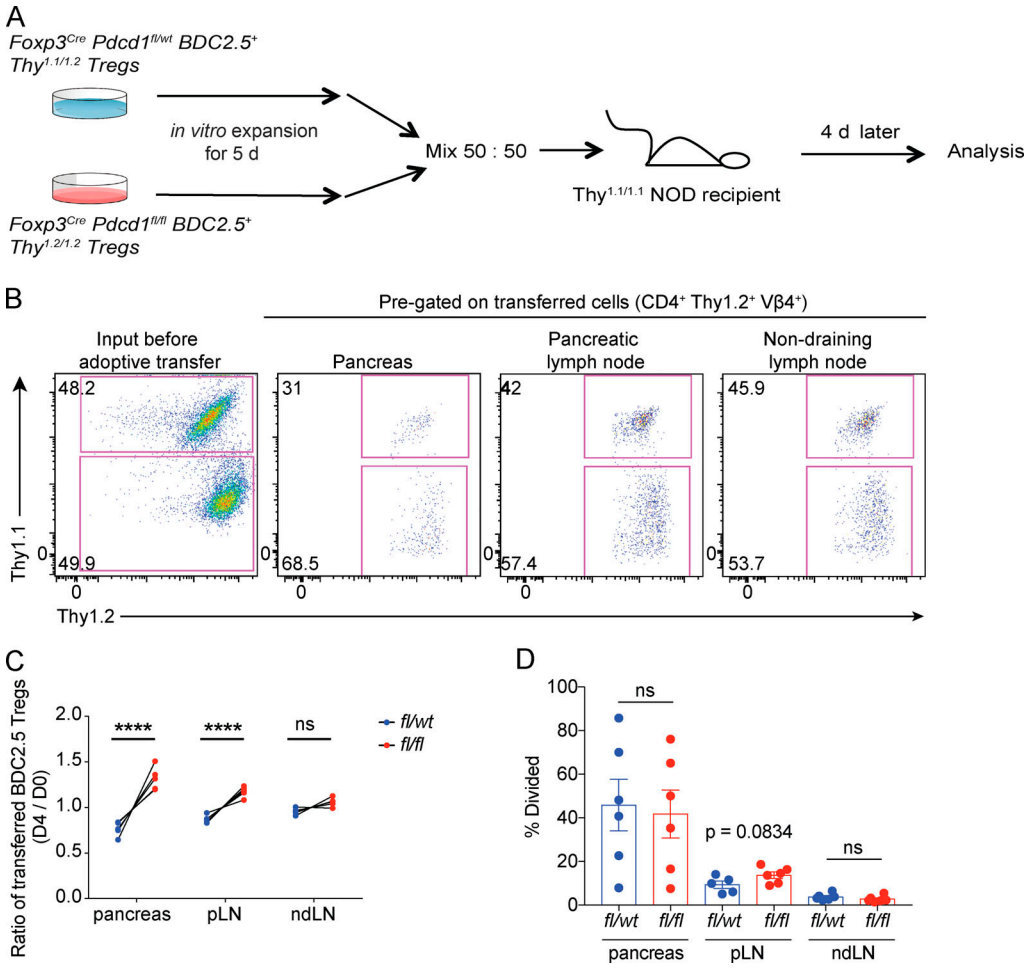

Figure 5. **PD-1–deficient BDC2.5 T reg cells have a competitive advantage compared with WT BDC2.5 T reg cells. (A)** Schematic of BDC2.5 T reg cell cotransfer experiment into NOD Thy1.1/Thy1.1 recipients. In this experiment, congenic markers are used to distinguish PD-1–deficient (Thy1.2 Thy1.2) and control (Thy1.1 Thy1.2) BDC2.5 T reg cells. **(B)** Representative flow cytometry plots of cotransferred PD-1–deficient BDC2.5 T reg cells (Thy1.2 Thy1.2) and littermate control BDC2.5 T reg cells (Thy1.1 Thy1.2) before adoptive transfer and 4 d after adoptive transfer into NOD Thy1.1/Thy1.1 recipients from pancreas, pLN, and ndLN. Transferred BDC2.5 T reg cells were pregated by $CD4^+$ $V\beta4^+$ $Thy1.2^+$ followed by subsetting by Thy1.1 to distinguish PD-1–deficient (Thy1.2 Thy1.2) and control (Thy1.1 Thy1.2) BDC2.5 T reg cells. **(C)** Quantification of adoptively transferred control BDC2.5 T reg cells (blue) and PD-1–deficient BDC2.5 T reg cells (red) from the pancreas, pLN, and ndLN of donor recipients (n = 4) at day 4 after transfer. The ratios were calculated by comparing frequencies of control BDC2.5 T reg cells at day 4 versus day 0 and PD-1–deficient BDC2.5 T reg cells at day 4 versus day 0. **(D)** Proliferation of WT BDC2.5 T reg cells (blue, n = 6) and PD-1–deficient BDC2.5 T reg cells (red, n = 6) from pancreas, pLN, and ndLN at day 4 after transfer. Data are representative of five independent experiments (B and C) or three independent experiments (D). Data are shown as means ± SEM. Significance was assessed using Student's t test in C and D. ****, $P < 0.001$. ns, not significant.

We compared ECAR in activated WT and PD-1–deficient T reg cells following the addition of three components: (1) glucose; (2) oligomycin to block mitochondrial ATP synthase, allowing for maximal glycolysis; and (3) 2-DG, a glucose analogue that inhibits glycolysis, to return ECAR to basal level and ensure changes in ECAR were due to glycolysis alone. Activated PD-1–deficient T reg cells had reduced ECAR as compared with activated WT T reg cells upon the addition of glucose and oligomycin (Fig. 7 A). Moreover, activated PD-1–deficient T reg cells had reduced glycolytic capacity (the maximum ECAR following addition of oligomycin; Fig. 7 B) and glycolytic reserve (the difference between the maximum ECAR upon addition of oligomycin and ECAR before addition of oligomycin; Fig. 7 C). These findings indicate that activated PD-1–deficient T reg cells are less glycolytic than activated WT T reg cells. Our observations are consistent with the reduced activation of the PI3K–AKT pathway in PD-1–deficient T reg cells, as activation of the PI3K–AKT pathway promotes glycolysis (Hu et al., 2016).

We also compared the mitochondrial functions of WT and PD-1–deficient T reg cells using a mitochondrial stress test to examine mitochondrial respiration as measured by the oxygen consumption rate (OCR). For these studies, we purified WT and PD-1–deficient T reg cells from the spleens of unmanipulated $Foxp3^{GFP}$ and $Pdcd1^{-/-}$ $Foxp3^{GFP}$ mice using $CD4^+$ FOXP3.GFP^+ and stimulated the T reg cells in vitro with plate-bound anti-CD3, anti-CD28, and 500 U/ml IL-2 for 16 h. Activated WT and PD-1–deficient T reg cells were sequentially treated with oligomycin, carbonyl cyanide–4(trifluoromethoxy) phenylhydrazone (FCCP; a mitochondrial uncoupler to allow for maximal oxygen consumption), and a mix of rotenone (complex I inhibitor) and

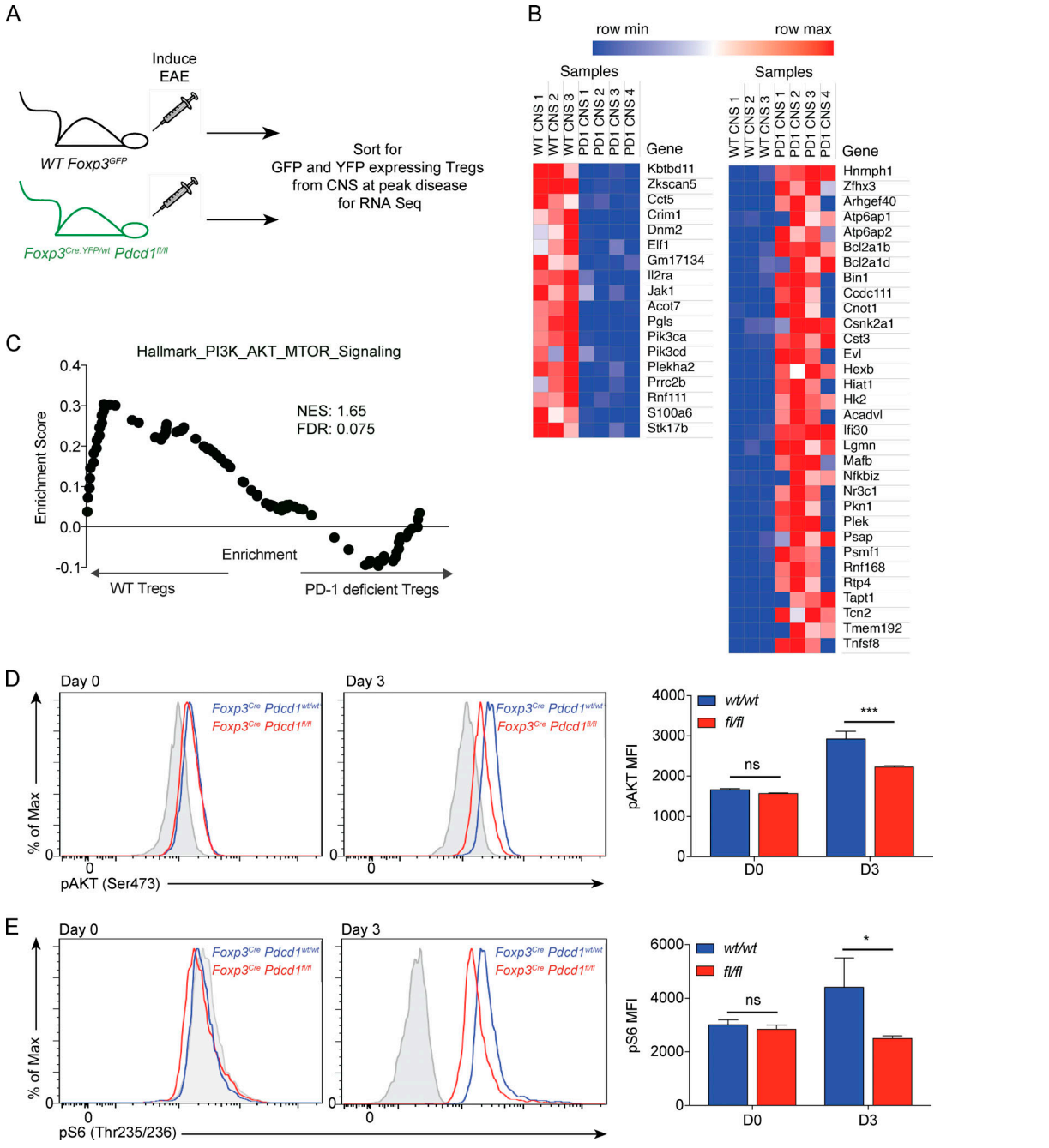

Figure 6. **PD-1–deficient T reg cells exhibit alterations in the PI3K–AKT pathway. (A)** Schematic of EAE experiment for RNA-seq analysis. *Foxp3*^{GFP} (green, *n* = 4) and *Foxp3*$^{Cre.YFP/wt}$ *Pdcd1*$^{fl/fl}$ (black, *n* = 4) mice were immunized to induce EAE. T reg cells were sorted from CNS at peak of disease to conduct RNA-seq analysis. **(B)** Heat map of differentially expressed genes between WT and PD-1–deficient T reg cells. **(C)** Gene set enrichment analysis of WT and PD-1–deficient T reg cells. FDR, false discovery rate; NES, normalized enrichment score. **(D)** Representative histogram of expression levels of pAKT (left) with summary of quantification of pAKT (right) in WT (blue, *n* = 4) and PD-1–deficient T reg cells (red, *n* = 4) during a T reg cell in vitro suppression assay at indicated time points. YFP-expressing T reg cells were sorted from *Foxp3*$^{Cre\text{-}YFP}$ *Pdcd1*$^{fl/fl}$ and littermate control *Foxp3*$^{Cre\text{-}YFP}$ *Pdcd1*$^{wt/wt}$ mice for the T reg cell in vitro suppression assays. **(E)** Representative histogram of expression levels of pS6 (left) with summary of quantification of pS6 levels (right) in WT (blue, *n* = 4) and PD-1–deficient T reg cells (red, *n* = 4) during a T reg cell in vitro suppression assay as in E at the indicated time points. RNA-seq was conducted once with biological replicates (*Foxp3*^{GFP} control, *n* = 3 and *Foxp3*$^{Cre.YFP/wt}$ *Pdcd1*$^{fl/fl}$, *n* = 4). Phospho-flow cytometry analysis and T reg cell–mediated in vitro suppression assay data are representative of three independent experiments. Data are shown as means ± SEM. Significance was assessed using a Student's *t* test (D and E). *, P < 0.05; ***, P < 0.005. ns, not significant.

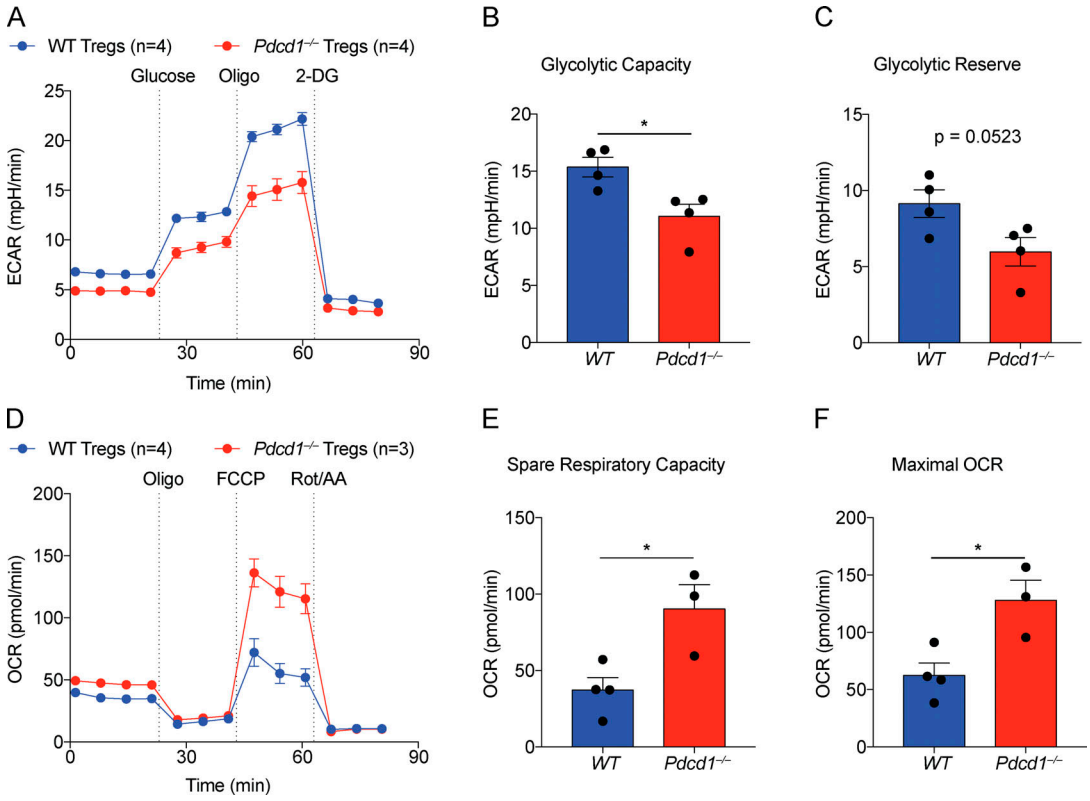

Figure 7. **PD-1–deficient and WT T reg cells have distinct bioenergetics profiles. (A–F)** ECAR (A–C) and OCR (D–F) measurement of activated splenic WT (blue, *n* = 4) and PD-1–deficient T reg cells (red, *n* = 4). WT and PD-1–deficient T cells were sort-purified from the spleens of unmanipulated *Foxp3*^{GFP} and *Pdcd1*$^{-/-}$ *Foxp3*^{GFP} mice using CD4^{+} GFP^{+} and stimulated with plate-bound anti-CD3, anti-CD28, and IL-2 in vitro for 16 h. **(A–C)** To assess ECAR, activated splenic T reg cells were replated in XF media and then treated with glucose, oligomycin, and 2-DG (treatment time indicated by vertical dotted lines) during the glycolysis stress test (A) using an extracellular flux analyzer. Glycolytic capacity (B) and glycolytic reserve (C) of WT (blue, *n* = 4) and PD-1–deficient T reg cells (red, *n* = 4) were determined. **(D-F)** To evaluate OCR, activated splenic WT (blue, *n* = 4) and PD-1–deficient T reg cells (red, *n* = 3) were replated in XF media and then treated with oligomycin, FCCP, and 2-DG (treatment time indicated by vertical dotted lines) during a mito stress test as measured by extracellular flux analyzer. Spare respiratory capacity (E) and maximal OCR (F) of WT (blue, *n* = 4) and PD-1–deficient T reg cells (red, *n* = 3) were determined. Data are representative of three independent experiments. Data are shown as means ± SEM. Significance was assessed using a Student's *t* test (B and D–F). *, P < 0.05.

antimycin A (complex III inhibitor) to terminate mitochondrial respiration. The addition of FCCP led to a significant increase in OCR in activated PD-1–deficient T reg cells as compared with activated WT T reg cells (Fig. 7 D). Activated PD-1–deficient T reg cells also had increased spare respiratory capacity, as calculated by the difference between maximum and basal respiration, (Fig. 7 E), and a significantly increased maximal respiratory capacity, as indicated by the maximum OCR upon the addition of FCCP (Fig. 7 F). Thus, compared with activated WT T reg cells, activated PD-1–deficient T reg cells have enhanced mitochondrial functions and are less glycolytic, a bioenergetic state associated with enhanced T reg cell suppressive capacity.

AKT activator reverses the enhanced suppressive activity of PD-1–deficient T reg cells

Several studies have demonstrated that activation of AKT results in reduced T reg cell suppressive capacity (Crellin et al., 2007; Gerriets et al., 2016). Since PD-1 deficiency in T reg cells down-regulates the PI3K–AKT pathway, we hypothesized that reduced PI3K–AKT pathway signaling in PD-1–deficient T reg cells contributes to their enhanced suppressive capacity. To test this hypothesis, we used an AKT activator that binds the plecktrin homology domain of AKT and causes AKT to adopt a conformation favorable for phosphorylation, thereby enhancing AKT activity (Jo et al., 2012). Treatment of WT T reg cells with this AKT activator up-regulates pAKT (Fig. 8 A), as expected, as well as pS6 (Fig. 8 B), indicating that the AKT activator is stimulating the PI3K–AKT pathway. We pretreated *Foxp3*^{Cre} *Pdcd1*$^{fl/wt}$ and *Foxp3*^{Cre} *Pdcd1*$^{fl/fl}$ T reg cells with the AKT activator and assessed their suppressive capacity using an in vitro suppression assay, as in Fig. 6. As expected, PD-1–deficient T reg cells had a higher suppressive capacity than WT T reg cells (Fig. 8, C and D, DMSO control). Pretreatment with the AKT activator reduced the suppressive capacity of *Foxp3*^{Cre} *Pdcd1*$^{fl/fl}$ T reg cells to the level of WT T reg cells (Fig. 8, C and D). These findings demonstrate reduced signaling through the PI3K–AKT pathway as a mechanism underlying the enhanced suppressive capacity of PD-1–deficient T reg cells.

Discussion

The PD-1 pathway plays multifaceted roles in T cell tolerance. PD-1 inhibitory signals raise the threshold for initial activation of naive self-reactive T cells and limit responses of self-reactive

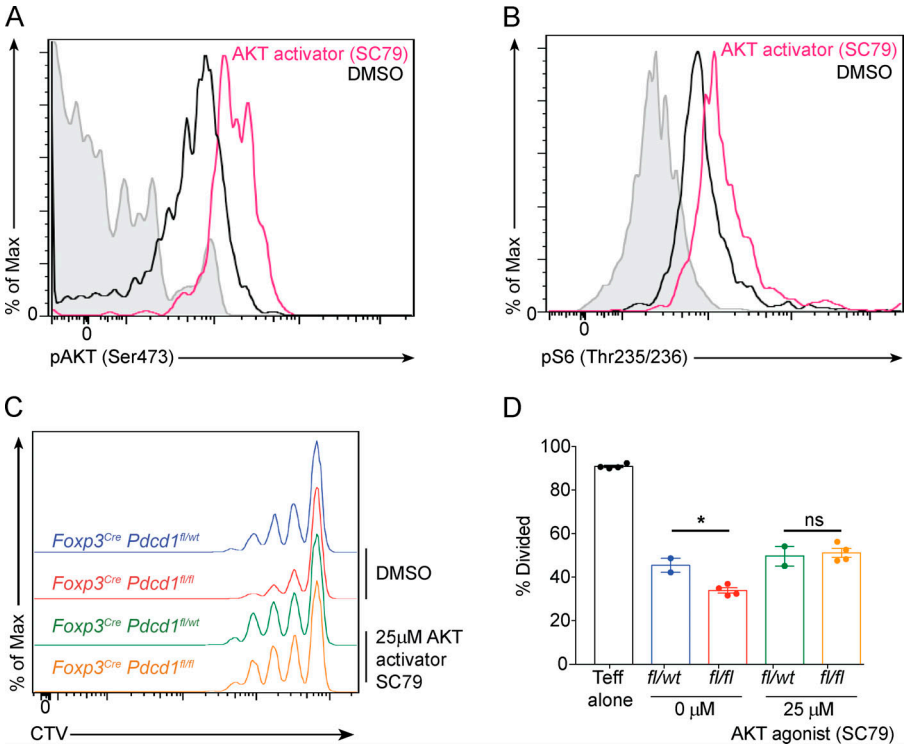

Figure 8. **AKT activator reverses enhanced suppressive function of PD-1–deficient T reg cells. (A and B)** Representative histogram of expression levels of pAKT (left) and (B) pS6 (right) in sorted splenic WT T reg cells treated with DMSO (black) or 25 μM AKT activator (pink) at 37°C for 1 h. **(C)** Representative histogram of Teff cells proliferation as measured with CTV dilution during an in vitro T reg cell–mediated suppression assay in which sort-purified control *Foxp3*^{Cre} *Pdcd1*$^{wt/wt}$ T reg cells (n = 2) treated with DMSO (blue) or 25 μM AKT activator (green) for 1 h or PD-1–deficient *Foxp3*^{Cre} *Pdcd1*$^{fl/fl}$ T reg cells (n = 4) treated with DMSO (red) or 25 μM AKT activator (orange) for one hour were washed twice and then co-cultured with WT Teff in the presence of irradiated APCs and stimulated with 1 μg/ml of anti-CD3 for 3–4 d. **(D)** Quantification of Teff cells proliferation as measured by CTV dilution during in vitro T reg-mediated suppression assay as described in C. Data are representative of three independent experiments. Data are shown as means ± SEM. Significance was assessed using a Student's t test. *, P < 0.05. ns, not significant.

Teff cells (Francisco et al., 2010). PD-L1 on nonhematopoietic cells mediates tissue tolerance, protecting target organs from attack by self-reactive T cells and immune-mediated damage (Barber et al., 2006; Keir et al., 2006; Reynoso et al., 2009; Scandiuzzi et al., 2014). Our studies using mice that lack PD-1 selectively on T reg cells establish a new mechanism by which the PD-1 pathway regulates T cell tolerance. Selective PD-1 deficiency in T reg cells increases their suppressive function, resulting in attenuated autoimmunity in EAE and NOD models. Thus, PD-1–mediated inhibition of T reg cells regulates T cell tolerance.

PD-1 is expressed in a variety of T cell types as well as natural killer cells and B cells. In PD-1$^{-/-}$ mice, PD-1 is deleted in all cells. Our *Foxp3*^{Cre} *Pdcd1*$^{fl/fl}$ mice enabled us to analyze how PD-1 regulates T reg cell function in vivo without potential confounding effects of PD-1 deficiency in other hematopoietic cells. Moreover, *iFoxp3*^{Cre} *Pdcd1*$^{fl/fl}$ mice allowed us to study PD-1 function in mature T reg cells, circumventing potential effects of PD-1 on selection of the T cell repertoire in the thymus. Zhang et al. reported that breeding PD-1–deficient mice with *IRES-GFPCre* reporter knock-in mice (Miyao et al., 2012) resulted in lethal pancreatitis in all male mice with the genotype *Foxp3-GFPCre* PD-1$^{-/-}$ by 3 mo of age (Zhang et al., 2016). While reduced FOXP3 expression in T reg cells contributed to this phenotype, these studies pointed to a role for PD-1 in limiting T reg cell function (Zhang et al., 2016). Our mice that selectively lack PD-1 in T reg cells demonstrate that PD-1 exerts cell-intrinsic inhibitory effects in T reg cells in the absence of effects related to T cell development or PD-1 deficiency in other cell types.

PD-1–deficient T reg cells limited Teff cell proliferation to a greater extent than WT T reg cells in in vitro suppression assays using different ratios of Teff cells to T reg cells, demonstrating that PD-1–deficient T reg cells are more suppressive than WT T reg cells on a per cell basis. Similar to our in vitro suppression assays, PD-1–deficient T reg cells suppressed in vivo Teff cell activation, expansion, and cytokine production more effectively than WT T reg cells in EAE and NOD diabetes, leading to less severe disease. We also observed an increase in the ratio of PD-1–deficient T reg cells relative to Teff cells in the target organs.

There are several potential explanations for the increase in T reg cell frequency in the target organ: enhanced T reg cell (1) expansion, (2) survival, (3) migration, and/or (4) stability. We examined each of these possibilities in the EAE model by assessing PD-1–deficient and PD-1^{+} T reg cells within the same microenvironment in *iFoxp3*^{Cre} *Pdcd1*$^{fl/fl}$ mice using a suboptimal dose of tamoxifen. This approach and the adoptive transfer experiments in the NOD diabetes model enabled analyses of PD-1–expressing and PD-1–deficient T reg cells in the same microenvironment and demonstrate the cell-intrinsic inhibitory function of PD-1 in T reg cells in two different autoimmune models of disease. These experiments point to increased expansion of PD-1–deficient T reg cells as an important mechanism leading to increased T reg cell presence in sites of disease (Fig. 3 and Fig. 5). We observed the greatest difference in Ki67 expression, a marker of proliferation, in splenic PD-1^{-} T reg cells compared with splenic PD-1^{+} T reg cells during EAE (Fig. 3 H and data not shown). This splenic expansion may be relevant to the clinical EAE phenotype observed since previous work reported that myelin-specific T cells expanding in the spleen migrate to the CNS during EAE (Flügel et al., 2001). These findings suggest that enhanced localized expansion of PD-1^{-} T reg cells in the spleen may contribute to the increased frequency of PD-1^{-}FOXP3^{+} T reg cells in the CNS. Similarly, our NOD studies also showed an increase in proliferation of PD-1–deficient T reg cells from

NOD.Foxp3^{Cre+} *Pdcd1*$^{fl/fl}$ *BDC2.5*$^{+}$ *Thy*$^{1.2}$ compared with control T reg cells from *NOD.Foxp3*$^{Cre+}$ *Pdcd1*$^{fl/wt}$ *BDC2.5*$^{+}$ *Thy*$^{1.1/1.2}$ mice in the pLN, further highlighting the importance of PD-1–mediated restraint on T reg cell expansion in a cell-intrinsic manner. We did not find significant differences in T reg cell survival by assessing Bcl-2 or cell death (data not shown) during EAE. In addition, there was neither increased T reg cell egress from the draining LNs nor significant differences in the frequency of T reg cells expressing CXCR3 or CCR6 in PD-1–deficient versus control T reg cells during EAE (data not shown). These data suggest that alterations in T reg cell migration are not the major mechanism underlying increased T reg cell presence in the CNS during EAE. We also used *Foxp3*^{Ert2CreGFP} *Pdcd1*$^{fl/fl}$ Rosa26^{LoxSTOPLoxTdtomato} reporter mice to examine T reg cell stability and found that PD-1 deleted T reg cells are not more stable than PD-1–expressing T reg cells (data not shown), suggesting that increased stability is also not the mechanism behind the increased frequency of PD-1–deficient T reg cells in the CNS. Thus, while the PD-1–deleted T reg cells may be expanding more, they also may be surviving less due to overstimulation and cell death. This mechanism may explain the similar absolute cell numbers of control and PD-1–deleted T reg cells in the CNS of control and *iFoxp3*^{Cre} *Pdcd1*$^{fl/fl}$ mice during EAE. It is ultimately the balance between the T reg cells and Teff cells that determines disease outcome and the enhanced frequency of highly suppressive T reg cells in the CNS of *iFoxp3*^{Cre} *Pdcd1*$^{fl/fl}$ mice is what attenuates severity of autoimmune disease in the EAE model.

We identified reduced signaling through the PI3K–AKT pathway as one mechanism underlying the increased suppressive capacity of PD-1–deleted T reg cells. Down-regulation of the PI3K–AKT pathway is critical for T reg cell development and optimal T reg cell suppressive function in vitro and in vivo (Haxhinasto et al., 2008; Crellin et al., 2007; Gerriets et al., 2016; Sauer et al., 2008). pAKT was reduced in PD-1–deficient T reg cells. By using an AKT activator, we demonstrated that the enhanced suppressive capacity in PD-1–deficient T reg cells could be overcome in vitro by increasing AKT signaling. These data suggest that PD-1 promotes signaling through the PI3K–AKT pathway in T reg cells. In contrast, PD-1 inhibits the activation of the PI3K–AKT pathway through attenuation of TCR- and CD28-mediated signaling and activation of PTEN during the activation of naive T cells (Patsoukis et al., 2013; Sheppard et al., 2004; Kamphorst et al., 2017; Hui et al., 2017). The distinct effects of PD-1 on the PI3K–AKT pathway during activation of naive T cells versus T reg cells likely reflect differential signaling requirements between the two cell types (Mikami and Sakaguchi, 2014; Yan et al., 2015; Franckaert et al., 2015).

There is a growing appreciation that metabolic reprogramming is critical for optimal T cell differentiation and effector functions (MacIver et al., 2013; Buck et al., 2015). Signals through PD-1 can modulate bioenergetics by inhibiting glycolysis and promoting fatty acid oxidation during activation of naive T cells (Patsoukis et al., 2015). We found that PD-1–deficient T reg cells have reduced glycolysis, a bioenergetic state that leads to increased T reg cell suppressive capacity. Our findings are in accordance with recent work demonstrating that glycolytic T reg cells have diminished suppressive capacity (Huynh et al., 2015; Gerriets et al., 2016). PD-1–deficient T reg cells also exhibit increased mitochondrial functions, which may result from activation of the AMPK pathway, known to promote mitochondrial oxidative metabolism and suppress glycolysis (Kishton et al., 2016; Blagih et al., 2015; Price et al., 2012). Our work highlights a previously unappreciated link between metabolism and PD-1 function in T reg cells.

The increased frequencies of CTLA-4 and TIGIT-expressing T reg cells in *Foxp3*^{Cre} *Pdcd1*$^{fl/fl}$ mice also may contribute to their enhanced suppressive capacity. CTLA-4 is a key mediator of T reg cell suppressive function (Wing et al., 2008). TIGIT expression defines a T reg cell subset with an activated phenotype and contributes to selective T reg cell–mediated suppression of proinflammatory type 1 and type 17 T helper cells by inducing secretion of the soluble effector molecule fibrinogen-like protein 2 (Fgl2; Joller et al., 2014).

The ameliorated EAE and diabetes in mice lacking PD-1 only in T reg cells contrast with the exacerbated EAE in *Pdcd1*$^{-/-}$ mice (Kroner et al., 2009; Salama et al., 2003; Wang et al., 2009) and the rapid diabetes in *NOD.Pdcd1*$^{-/-}$ mice (Wang et al., 2005; Ansari et al., 2003; Paterson et al., 2011; Keir et al., 2006). The distinct outcomes of selective PD-1 deficiency in T reg cells versus global PD-1 deficiency point to distinct immunoregulatory functions for PD-1 on different cell types. Our findings underscore the importance of understanding the consequences of PD-1 inhibitory signals in different cell types and determining how they are integrated to regulate the outcome of an immune response. PD-1 immunotherapy inhibits PD-1 signals in all cell types, but the integrated outcome is enhanced T cell functions in tumors that respond to PD-1 cancer immunotherapy. Development of agents such as bispecific antibodies that target PD-1 on Teff cells, but not T reg cells, might be even more effective. Understanding how PD-1 signals in different cell types and inflammatory contexts is also important when considering the potential for autoimmune-mediated adverse events and the susceptibility of cancer patients to acute infections. This knowledge may provide insights into how to deliver PD-1 inhibitory signals to ameliorate autoimmune diseases or transplant rejection. Bispecific antibodies that target PD-1 on T reg cells may provide a means to deliver PD-1 inhibitory signals.

As PD-1 inhibits both T reg cells and CD4^{+} FOXP3^{-} Teff cells, this may explain why CTLA-4 immunotherapy, which works in part by decreasing T reg cell function, may synergize so well with PD-1 blockade for cancer immunotherapy (Selby et al., 2013; Simpson et al., 2013; Wolchok et al., 2013). Anti-CTLA-4 may reduce the number of T reg cells with enhanced function due to PD-1 blockade, thereby increasing antitumor Teff cell responses due to CTLA-4 and PD-1 blockade. Combining PD-1 blockade with other strategies that reduce T reg cell numbers or function also may be an effective combination strategy for cancer immunotherapy (Pardoll, 2012; Topalian et al., 2014).

In summary, our data provide novel insight into how the PD-1 pathway regulates T cell tolerance. We have shown that PD-1 inhibitory signals limit T reg cell activation and suppressive capacity. PD-1 control of T reg cells is a mechanism by which PD-1 regulates T cell tolerance. Our findings demonstrate that

PD-1 is an "equal-opportunity" inhibitor of T cell activities. When PD-1 is lost on cells whose primary function is to suppress immune responses, the consequence is a stronger suppressor cell.

Materials and methods

Mice

WT Foxp3^{GFP} reporter, *Pdcd1*$^{-/-}$ *Foxp3*^{GFP}, *Foxp3*$^{Cre\text{-}YFP}$ mice, and *Foxp3*$^{ERT2\text{-}Cre\text{-}GFP}$ mice have been previously reported (Rubtsov et al., 2008). *TCRα*$^{-/-}$, *CD45.1 C57Bl/6* mice and *Thy1.1 NOD* mice were obtained from The Jackson Laboratory. To create PD-1 conditional knockout mice, we generated a PD-1 targeting vector containing frt sites on either side of a selection cassette containing the neo gene under control of the PGK promoter. Exons 2, 3, and 4, encoding the IgV, transmembrane, and first cytoplasmic exon of PD-1, respectively, were inserted into the vector downstream of the selection cassette. The flanking regions of the PD-1 gene were cloned from a PD-1 containing bacterial artificial chromosome using standard techniques. Linearized vector DNA was electroporated into Bruce 4 C57BL/6 embryonic stem (ES) cells and the resulting neomycin-resistant ES cells were screened for homologous recombination. ES cells carrying the desired recombinant event were microinjected into blastocysts, and the resulting chimeric mice gave germline transmission of the targeted PD-1 allele. Mice carrying the targeted allele were bred with Flpe-expressing mice to delete neo, yielding PD-1 conditional knockout mice (*Pdcd1*$^{fl/fl}$ mice) with exons 2, 3, and 4 flanked by loxP sites. These mice were bred to *Foxp3*$^{Cre\text{-}yfp}$ (referred to as *Foxp3*^{Cre} *Pdcd1*$^{fl/fl}$ mice) or *Foxp3*$^{ERT2\text{-}Cre\text{-}GFP}$ (referred to as *iFoxP3*^{Cre} *Pdcd1*$^{fl/fl}$ mice) mice to generate mice that selectively eliminate PD-1 in FoxP3-expressing cells constitutively or inducibly. To control for changes in FOXP3 expression due to the knock-in Cre alleles, *Foxp3*^{Cre} *Pdcd1*$^{wt/wt}$, or *iFoxp3*^{Cre} *Pdcd1*$^{wt/wt}$ were used as controls. The mice used in these studies were between 5 and 12 wk old, and littermates were used as controls and cohoused with PD-1–deficient mice before experiments. To inducibly delete PD-1, *iFoxp3*^{Cre} *Pdcd1*$^{fl/fl}$ mice or *iFoxp3*^{Cre} *Pdcd1*$^{wt/wt}$ control mice were given 1 mg tamoxifen (Sigma) in sunflower oil for 10 consecutive days i.p. for full dose or 5 consecutive days i.p. for half dose, followed by 5 d rest before experiments. For the NOD studies, *Pdcd1*$^{fl/fl}$ B6 mice were backcrossed onto the NOD background for 11 generations and then bred with *Foxp3*^{Cre} NOD mice (Zhou et al., 2008). Single-nucleotide polymorphism (SNP) analysis of 20 Idd loci covering 144 SNPs revealed that mice were 98.5% NOD Idd loci at the F9 generation. There were four heterozygous SNPs located on chromosome 1 within the Pdcd1 gene region from the targeted Pdcd1.B6 gene construct. NOD females were used for cellular analysis. All mice were maintained in a pathogen-free facility and used according to Harvard Medical School, University of Pittsburgh School of Medicine and National Institutes of Health guidelines. Harvard Medical School and the University of Pittsburgh School of Medicine are accredited by the American Association of Accreditation of Laboratory Animal Care.

Antibodies

Anti-CD3 (145-2C11) for in vitro functional studies was obtained from BioXCell. Conjugated anti-CD4 (RM4-5), anti-CD8β (YTS156.7.7), TCR-β (H57-597), Thy1.1 (OX-7), Thy1.2 (30-H12), anti-CD62L (MEL-14), anti-CD44 (IM7), anti-CTLA-4 (UC10-4B9), anti-PD-1 (RMP1-30), anti-PD-L1(10F.9G2), anti-GITR (DTA-1), anti-ICOS (C98.4A), anti-TIGIT (1G9), anti-LAP (TW7-16B4), anti-IL-10 (JES5-16E3), anti-IL-17A (TC11-18H10.1), and anti-IFN-γ (XMG1.2) were purchased from BioLegend. Anti-CD8β (H35-17.2), anti-Ki67 (B56), and anti-PTEN (A2B1) were from BD Biosciences. Anti-FoxP3 (FJK-16s) was purchased from eBioscience. pAKT (D9E), pS6 (D57.2.2E), and pFOXO1/O3A (9464) antibodies were purchased from Cell Signaling Technologies.

Flow cytometry analysis

Single-cell suspensions from spleen or LNs were prepared and resuspended in staining buffer (PBS containing 1% FBS and 2 mM EDTA) and stained with the indicated antibodies. For intracellular cytokine staining, cells were activated with PMA (Sigma) and ionomycin (Sigma) in the presence of Golgistop (BD Biosciences) for 4 h, followed by intracellular staining. For the detection of FOXP3, we used the FOXP3 staining kit from eBioscience and followed the manufacturer's protocol for intracellular staining. For PTEN, pAKT, pS6, and pFOXO1A/O3A staining, cells were fixed in 2% PFA (Affymetrix) for 20 min and permeabilized with 90% methanol overnight at −20°C. Cells were then washed and stained with pAKT, pS6, and pFOXO1A/O3A antibodies in eBioscience permeabilization buffer for an hour before flow cytometry analysis. Measurements of cytokines in culture supernatants were performed by cytometric bead array (CBA; BD Biosciences). Data were acquired on a LSRII (BD Biosciences) and analyzed with FlowJo software (Tree Star).

T cell sorting and in vitro T reg cell suppression assays

CD4$^+$ T cells were purified by positive selection (Miltenyi Biotec). For in vitro T reg cell–mediated suppression assays, CD4$^+$ T reg cells were sorted as CD4$^+$FOXP3$^+$ (using the YFP reporter). CD62L$^+$ CD4$^+$ FOXP3$^-$ (using either GFP or YFP reporter) cells were sorted as Teff cells. 10^5 Teff cells and the indicated ratios of T reg cells were stimulated using irradiated splenocytes from *TCRα*$^{-/-}$ mice as APCs using a 4–5:1 ratio of APCs to Teff cells and 1 µg /ml anti-CD3 mAb. Cells were cultured in RPMI 1640 (Invitrogen) supplemented with 10% FBS, 2 mM L-glutamine, 10 mM Hepes, 1% penicillin/streptomycin, and 50 µM β-mercaptoethanol for 3–4 d, after which culture supernatants were collected for analyses of cytokine production (see Flow cytometry analysis). For CellTrace Violet (CTV) labeling of Teff cells, we used the CTV Cell Proliferation Kit (Thermo Fisher Scientific) and followed the manufacturer's protocol. For in vitro T reg cell–mediated suppression assays using AKT activator (SC79; Sigma), sorted T reg cells were incubated with 25 µM AKT activator or DMSO control for 1 h at 37°C, washed twice, and then cultured as described.

In vitro T reg cell differentiation assays

Naive CD4 T cells (CD62L$^+$ FOXP3$^-$) were sorted from *Foxp3*$^{Cre\text{-}YFP}$ *Pdcd1*$^{fl/fl}$ mice or *Foxp3*$^{Cre\text{-}YFP}$ *Pdcd1*$^{wt/wt}$ control mice using the YFP reporter and plated at 1 × 10^6/ml in 24-well plates coated with 10 µg/ml anti-CD3 and 2 µg/ml of anti-CD28 in the presence of 50 U/ml human IL-2 (ProSpec) with or without

2.5 ng/ml TGF-β (R&D Systems) for 4 d. After 4 d in culture, cells were analyzed for FoxP3 expression by flow cytometry.

Induction of EAE

Mice were immunized with 100 µg MOG_{35-55} in CFA (supplemented with 2 mg/ml heat-killed *Mycobacterium tuberculosis* H37RA) in both flanks and given 200 ng pertussis toxin i.p. on days 0 and 2. Mice were monitored for signs of clinical disease and scored as follows: 1, limp tail; 2, weak gait; 3, hindlimb paralysis; 4, hindlimb and forelimb paralysis; and 5, moribund. For analyses of cellular infiltrates in the CNS, brain and spinal cords were isolated at peak disease, unless otherwise specified in the text, and resuspended in 30% Percoll/PBS and overlaid above a 70% Percoll gradient. Following centrifugation, lymphocytes in the interface were removed, washed, and resuspended in culture medium for analysis.

Measurement of diabetes and insulitis

Diabetes and insulitis were assessed as previously described (Paterson et al., 2011). Briefly, mice were monitored weekly for high urine glucose by Diastix (Diastix; Bayer). Mice positive by Diastix were confirmed by blood glucose measurement (Ascensia Contour; Bayer). Diabetes was confirmed by blood glucose level of ≥250 mg/dl. For histology, pancreata were fixed in 10% buffered formalin overnight, embedded in paraffin, and stained with hematoxylin and eosin. Islets were scored in blinded fashion as follows: 0, no infiltration; 1, perivascular/periductular infiltrates with lymphocytes touching islet perimeters, but not penetrating; 2, lymphocytic penetration of up to 25% of islet mass; 3, lymphocytic penetration of up to 75% of islet mass; and 4, <20% of islet mass remaining. Photomicrographs were taken with a mounted digital camera (Olympus DP71) driven by Olympus DP Controller software. Images were prepared using Adobe Photoshop and Illustrator CS3 (Adobe Systems).

Isolation of lymphocytes from pancreas

For cellular analysis of lymphocytes from pancreata, mice were perfused with 10 ml PBS. Pancreata were removed, dissociated with mechanical forces (gentleMACS dissociator; Miltenyi Biotec), and incubated in digestion media (Collagenase IV and DNaseI; Sigma) in a 37°C water bath for 20 min. The digested tissues were filtered through 70-µm strainers (BD Biosciences), washed with media, and resuspended in 44% Percoll/PBS. The resulting cell suspension was overlaid with 67% Percoll and centrifuged at 700 *g* without brake. Following centrifugation, lymphocytes in the interface were isolated, washed, and resuspended in culture medium for analysis or stimulated for cytokine production.

T reg cell expansion and adoptive transfer

Congenically marked control *NOD.Foxp3*$^{Cre+}$ *Pdcd1*$^{fl/wt}$ *BDC2.5*$^{+}$ *Thy*$^{1.1/1.2}$ T reg cells and PD-1–deficient *NOD.Foxp3*$^{Cre+}$ *Pdcd1*$^{fl/fl}$ *BDC2.5*$^{+}$ *Thy*$^{1.2/1.2}$ T reg cells were sorted from spleens as TCR-β^{+} CD4^{+} FoxP3.GFP^{+} cells, activated with PMA (0.1 µg/ml; Sigma) and ionomycin (0.5 µg/ml; Sigma) with human IL-2 (1,000 U/ml; Prometheus) for 2 d, and then expanded for another 3 d with human IL-2. WT and PD-1–deficient T reg cells were mixed at an equal ratio and adoptively cotransferred into 6- to 10-wk-old *NOD Thy*$^{1.1/1.1}$ recipients (2 × 10^6 total T reg cells). *Thy1.1 NOD* recipients were sacrificed and analyzed 4 d after transfer.

Metabolic studies

The ECAR and OCR were measured by the glycolysis stress test and mito stress test, respectively, using a XF96 extracellular flux analyzer (Agilent Technologies and Seahorse Bioscience). CD4^{+} T reg cells were sorted from the spleens of unmanipulated *Foxp3*^{GFP} and *Pdcd1*$^{-/-}$ *Foxp3*^{GFP} mice using CD4^{+} and FOXP3.GFP^{+}. Sorted splenic T reg cells were activated with plate-bound anti-CD3 (5 µg/ml) and anti-CD28 (5 µg/ml) in the presence of IL-2 (500 U/ml; ProSpec) for 16 h. 1 × 10^5 T reg cells were plated in XF Assay media onto a 96-well XF plate coated with CellTak (CN 354240; BD Biosciences), followed by the sequential addition of glucose (10 mM), oligomycin (1 µM), and 2-deoxy glucose (50 mM). The mito stress test was performed with XF assay medium and consisted of the sequential addition of oligomycin (1 µM), FCCP (1.5 µM), and finally rotenone (100 nM) and antimycin (1 µM).

RNA-seq

RNA-seq library preparations were performed as described previously (Sage et al., 2016). In brief, RNA isolation was performed using MyOne Silane Dynabeads (Thermo Fisher Scientific) and followed by fragmentation and barcoding of RNA using 8-bp barcodes in conjunction with standard Illumina adaptors. Primers were removed using Agencourt AMPure XP bead cleanup (Beckman Coulter/Agencourt), and samples were amplified with 14 PCR cycles. Libraries were gel purified and quantified using a Qubit high-sensitivity DNA kit (Invitrogen), and library quality was confirmed using Tapestation high-sensitivity DNA tapes (Agilent Technologies). RNA-seq reactions were performed on an Illumina HiSeq 2000 or Illumina NextSeq sequencer (Illumina) according to the manufacturer's instructions, sequencing 50-bp reads. Analysis was performed using the CLC Genomics Workbench version 8.0.1 RNA-seq analysis software package (Qiagen). Briefly, reads were aligned (mismatch cost = 2, insertion cost = 3, deletion cost = 3, length fraction = 0.8, and similarity fraction = 0.8) to the mouse genome, and differential gene expression analysis was performed (total count filter cutoff = 5.0). Results were normalized to reads per million. Morpheus (Broad Institute) was used to generate heat maps. For gene set enrichment analysis, RNA-seq data were converted to human nomenclature and compared with GSEA Hallmark mSigDatabases using standard settings (Broad Institute).

Data availability

RNA-seq transcriptome data have been deposited in the Gene Expression Omnibus database repository (accession no. GSE155956).

Statistical analysis

All of the statistical analyses were performed using Prism software, version 6 (GraphPad). Results are presented as mean ± SEM and significance was determined using either unpaired two-tailed Student's *t* test or Mann–Whitney nonparametric test. Asterisks denote level of statistical significance (*, P < 0.05; **, P < 0.01; and ***, P < 0.001).

Online supplemental material

Fig. S1 describes the generation and characterization of mice lacking PD-1 on T reg cells. Fig. S2 describes the generation of iT reg cells from conditional knockout mice lacking PD-1 specifically on T reg cells. Fig. S3 shows the immune characterization of NOD mice lacking PD-1 specifically on T reg cells. Fig. S4 shows the transcriptional analysis of WT and PD-1–deficient T reg cells. Table S1 shows the gene set enrichment analysis comparing WT and PD-1–deficient T reg cells.

Acknowledgments

We thank Qian Zhan for assistance with histopathology of the pancreas from NOD mice; Xiaohui He, Valeria Rosado, and Christian Rodriguez for mouse colony maintenance; Bhavana Priyaharshini and Alison Moreno for technical support for the metabolic seahorse assay; and Larry Turka for valuable insights and discussions.

This work was supported by a National Institutes of Health Ruth L. Kirschstein National Research Service Award 1F31 DK105624-01A1 to C.L. Tan, National Institute of General Medical Sciences award T32GM007753 to J.R. Kuchroo, a National Science Foundation graduate fellowship to V.R. Juneja, a National Institutes of Health fellowship to P.T. Sage (5T32HL007627), a National Multiple Sclerosis Society fellowship to S.B. Lovitch, and National Institutes of Health grants P01 AI56299 (to A.H. Sharpe, G.J. Freeman, P.T. Sage, and B.R. Blazar), P50CA101942-11A1 (to A.H. Sharpe and G.J. Freeman), P01 AI39671 (to A.H. Sharpe), R37AI38310 (to A.H. Sharpe), R01 HL11879 and R37 AI34495 (to B.R. Blazar), R01 DK089125 and R01 AI144422 (to D.A.A. Vignali), and P01 AI108545 (to D.A.A. Vignali and A.H. Sharpe).

Author contributions: C.L. Tan, J.R. Kuchroo, and L.M. Francisco designed and performed most of the experiments, carried out statistical analyses, and wrote the manuscript. P.T. Sage sequenced RNA-cDNA libraries and performed initial data normalization. P.T. Sage, C.L. Tan, and J.R. Kuchroo performed computational analysis of the RNA-seq data. J. Buck assisted with NOD diabetes experiments, in vitro T reg cell–mediated suppression assays, and metabolic seahorse assays. D. Liang, S.L. McArdel, and Y.R. Thaker assisted with EAE experiments. G.J. Freeman designed and made the *Pdcd1*$^{fl/fl}$ construct, and S.J. Lee and S.B. Lovitch generated the *Foxp3*^{Cre} *Pdcd1*$^{fl/fl}$ mice. G.F. Murphy and C. Lian assisted with H&E staining of pancreas and scoring of islets. Q. Zhang monitored the *NOD.Foxp3*^{Cre} *Pdcd1*$^{fl/fl}$ mice for diabetes at the University of Pittsburgh. V.R. Juneja, D.A.A. Vignali, B.R. Blazar, and G.J. Freeman provided valuable insights and discussions. A.H. Sharpe and G.J. Freeman conceived the project. A.H. Sharpe directed the research and wrote the manuscript. All authors edited and approved the manuscript.

Disclosures: P.T. Sage reported a patent to PCT/US16/57031 pending. L.M. Francisco reported "other" from Evelo Biosciences and GlaxoSmithKline outside the submitted work; in addition, L.M. Francisco had a patent to US Patent 10,577,586 pending, a patent to WO2017066561A2 pending, and a patent to US20150299322A1 with royalties paid; and is currently an employee of Evelo Biosciences. V.R. Juneja reported a patent number 20180303922 issued. B.R. Blazar reported grants from the National Institutes of Health and personal fees from BlueRock Therapeutics, Magenta Therapeutics, Kadmon Pharmaceuticals, Incyte Corp, Obsidian Therapeutics, Regeneron Pharmaceuticals, Regimmune, Dr. Reddy, and Equillium Inc. outside the submitted work. D.A.A. Vignali reported personal fees from Almirall outside the submitted work and reported, "cofounder and stock holder - Novasenta and Tizona; stock holder - Oncorus and Werewolf; patents licensed and royalties - Astellas, BMS; scientific advisory board member - Tizona, Werewolf and F-Star; consultant - Astellas, BMS, Almirall; research funding - BMS, Astellas and Novasenta." G.J. Freeman reported a patent with royalties paid (Roche); a patent with royalties paid (Merck MSD); a patent with royalties paid (Bristol-Myers Squibb); a patent with royalties paid (Merck KGA); a patent with royalties paid (Boehringer-Ingelheim); a patent with royalties paid (AstraZeneca); a patent with royalties paid (Dako); a patent with royalties paid (Leica); a patent with royalties paid (Novartis); and a patent with royalties paid (Mayo Clinic). G.J. Freeman has served on advisory boards for Roche, Bristol-Myers-Squibb, Xios, Origimed, Triursus, iTeos, NextPoint, IgM, Jubilant and GV20, and has equity in Nextpoint, Triursus, Xios, iTeos, IgM, and GV20. A.H. Sharpe reported personal fees from Surface Oncology, Sqz Biotech, Selecta, Elstar, and Elpiscience; "other" from Monopteros; grants from Novartis, Merck, Roche, Ipsen, UCB, and Quark Ventures outside the submitted work; and is on the scientific advisory boards for the Massachusetts General Cancer Center, Program in Cellular and Molecular Medicine at Boston Children's Hospital and the Human Oncology and Pathogenesis Program at Memorial Sloan Kettering Cancer Center and Scientific Editor for the Journal of Experimental Medicine. A.H. Sharpe reported the following patents: 7,432,059, with royalties paid (Roche, Merck, Bristol-Myers-Squibb, EMD-Serono, Boehringer-Ingelheim, AstraZeneca, Leica, Mayo Clinic, Dako and Novartis); 7,722,868, with royalties paid (Roche, Merck, Bristol-Myers-Squibb, EMD-Serono, Boehringer-Ingelheim, AstraZeneca, Leica, Mayo Clinic, Dako and Novartis); 8,652,465, licensed (Roche), 9,457,080, licensed (Roche); 9,683,048, licensed (Novartis); 9,815,898, licensed (Novartis); 9,845,356, licensed (Novartis); 10,202,454, licensed (Novartis); 10,457,733, licensed (Novartis); 9,580,684, issued; 9,988,452, issued; 10,370,446, issued. No other disclosures were reported.

Submitted: 3 December 2018
Revised: 30 June 2020
Accepted: 26 August 2020

References

Amarnath, S., C.W. Mangus, J.C. Wang, F. Wei, A. He, V. Kapoor, J.E. Foley, P.R. Massey, T.C. Felizardo, J.L. Riley, et al. 2011. The PDL1-PD1 axis converts human TH1 cells into regulatory T cells. *Sci. Transl. Med.* 3. 111ra120. https://doi.org/10.1126/scitranslmed.3003130

Ansari, M.J., A.D. Salama, T. Chitnis, R.N. Smith, H. Yagita, H. Akiba, T. Yamazaki, M. Azuma, H. Iwai, S.J. Khoury, et al. 2003. The programmed death-1 (PD-1) pathway regulates autoimmune diabetes in nonobese diabetic (NOD) mice. *J. Exp. Med.* 198:63–69. https://doi.org/10.1084/jem.20022125

Barber, D.L., E.J. Wherry, D. Masopust, B. Zhu, J.P. Allison, A.H. Sharpe, G.J. Freeman, and R. Ahmed. 2006. Restoring function in exhausted CD8

T cells during chronic viral infection. *Nature*. 439:682–687. https://doi.org/10.1038/nature04444

Blagih, J., F. Coulombe, E.E. Vincent, F. Dupuy, G. Galicia-Vázquez, E. Yurchenko, T.C. Raissi, G.J. van der Windt, B. Viollet, E.L. Pearce, et al. 2015. The energy sensor AMPK regulates T cell metabolic adaptation and effector responses in vivo. *Immunity*. 42:41–54. https://doi.org/10.1016/j.immuni.2014.12.030

Bluestone, J.A., H. Bour-Jordan, M. Cheng, and M. Anderson. 2015. T cells in the control of organ-specific autoimmunity. *J. Clin. Invest*. 125:2250–2260. https://doi.org/10.1172/JCI78089

Bour-Jordan, H., J.H. Esensten, M. Martinez-Llordella, C. Penaranda, M. Stumpf, and J.A. Bluestone. 2011. Intrinsic and extrinsic control of peripheral T-cell tolerance by costimulatory molecules of the CD28/ B7 family. *Immunol. Rev*. 241:180–205. https://doi.org/10.1111/j.1600-065X.2011.01011.x

Buck, M.D., D. O'Sullivan, and E.L. Pearce. 2015. T cell metabolism drives immunity. *J. Exp. Med*. 212:1345–1360. https://doi.org/10.1084/jem.20151159

Callahan, M.K., M.A. Postow, and J.D. Wolchok. 2016. Targeting T Cell Co-receptors for Cancer Therapy. *Immunity*. 44:1069–1078. https://doi.org/10.1016/j.immuni.2016.04.023

Chapman, N.M., and H. Chi. 2014. mTOR signaling, Tregs and immune modulation. *Immunotherapy*. 6:1295–1311. https://doi.org/10.2217/imt.14.84

Crellin, N.K., R.V. Garcia, and M.K. Levings. 2007. Altered activation of AKT is required for the suppressive function of human CD4+CD25+ T regulatory cells. *Blood*. 109:2014–2022. https://doi.org/10.1182/blood-2006-07-035279

Flies, D.B., B.J. Sandler, M. Sznol, and L. Chen. 2011. Blockade of the B7-H1/PD-1 pathway for cancer immunotherapy. *Yale J. Biol. Med*. 84:409–421.

Flügel, A., T. Berkowicz, T. Ritter, M. Labeur, D.E. Jenne, Z. Li, J.W. Ellwart, M. Willem, H. Lassmann, and H. Wekerle. 2001. Migratory activity and functional changes of green fluorescent effector cells before and during experimental autoimmune encephalomyelitis. *Immunity*. 14:547–560. https://doi.org/10.1016/S1074-7613(01)00143-1

Fontenot, J.D., M.A. Gavin, and A.Y. Rudensky. 2003. Foxp3 programs the development and function of CD4+CD25+ regulatory T cells. *Nat. Immunol*. 4:330–336. https://doi.org/10.1038/ni904

Francisco, L.M., V.H. Salinas, K.E. Brown, V.K. Vanguri, G.J. Freeman, V.K. Kuchroo, and A.H. Sharpe. 2009. PD-L1 regulates the development, maintenance, and function of induced regulatory T cells. *J. Exp. Med*. 206:3015–3029. https://doi.org/10.1084/jem.20090847

Francisco, L.M., P.T. Sage, and A.H. Sharpe. 2010. The PD-1 pathway in tolerance and autoimmunity. *Immunol. Rev*. 236:219–242. https://doi.org/10.1111/j.1600-065X.2010.00923.x

Franckaert, D., J. Dooley, E. Roos, S. Floess, J. Huehn, H. Luche, H.J. Fehling, A. Liston, M.A. Linterman, and S.M. Schlenner. 2015. Promiscuous Foxp3-cre activity reveals a differential requirement for CD28 in Foxp3^{+} and Foxp3^{-} T cells. *Immunol. Cell Biol*. 93:417–423. https://doi.org/10.1038/icb.2014.108

Gerriets, V.A., R.J. Kishton, M.O. Johnson, S. Cohen, P.J. Siska, A.G. Nichols, M.O. Warmoes, A.A. de Cubas, N.J. MacIver, J.W. Locasale, et al. 2016. Foxp3 and Toll-like receptor signaling balance T_{reg} cell anabolic metabolism for suppression. *Nat. Immunol*. 17:1459–1466. https://doi.org/10.1038/ni.3577

Haxhinasto, S., D. Mathis, and C. Benoist. 2008. The AKT-mTOR axis regulates de novo differentiation of CD4+Foxp3+ cells. *J. Exp. Med*. 205:565–574. https://doi.org/10.1084/jem.20071477

Hori, S., T. Nomura, and S. Sakaguchi. 2003. Control of regulatory T cell development by the transcription factor Foxp3. *Science*. 299:1057–1061. https://doi.org/10.1126/science.1079490

Hu, H., A. Juvekar, C.A. Lyssiotis, E.C. Lien, J.G. Albeck, D. Oh, G. Varma, Y.P. Hung, S. Ullas, J. Lauring, et al. 2016. Phosphoinositide 3-Kinase Regulates Glycolysis through Mobilization of Aldolase from the Actin Cytoskeleton. *Cell*. 164:433–446. https://doi.org/10.1016/j.cell.2015.12.042

Hui, E., J. Cheung, J. Zhu, X. Su, M.J. Taylor, H.A. Wallweber, D.K. Sasmal, J. Huang, J.M. Kim, I. Mellman, et al. 2017. T cell costimulatory receptor CD28 is a primary target for PD-1-mediated inhibition. *Science*. 355:1428–1433. https://doi.org/10.1126/science.aaf1292

Huynh, A., M. DuPage, B. Priyadharshini, P.T. Sage, J. Quiros, C.M. Borges, N. Townamchai, V.A. Gerriets, J.C. Rathmell, A.H. Sharpe, et al. 2015. Control of PI(3) kinase in Treg cells maintains homeostasis and lineage stability. *Nat. Immunol*. 16:188–196. https://doi.org/10.1038/ni.3077

Jo, H., S. Mondal, D. Tan, E. Nagata, S. Takizawa, A.K. Sharma, Q. Hou, K. Shanmugasundaram, A. Prasad, J.K. Tung, et al. 2012. Small molecule-induced cytosolic activation of protein kinase Akt rescues ischemia-elicited neuronal death. *Proc. Natl. Acad. Sci. USA*. 109:10581–10586. https://doi.org/10.1073/pnas.1202810109

Joller, N., E. Lozano, P.R. Burkett, B. Patel, S. Xiao, C. Zhu, J. Xia, T.G. Tan, E. Sefik, V. Yajnik, et al. 2014. Treg cells expressing the coinhibitory molecule TIGIT selectively inhibit proinflammatory Th1 and Th17 cell responses. *Immunity*. 40:569–581. https://doi.org/10.1016/j.immuni.2014.02.012

Josefowicz, S.Z., L.F. Lu, and A.Y. Rudensky. 2012. Regulatory T cells: mechanisms of differentiation and function. *Annu. Rev. Immunol*. 30:531–564. https://doi.org/10.1146/annurev.immunol.25.022106.141623

Juneja, V.R., K.A. McGuire, R.T. Manguso, M.W. LaFleur, N. Collins, W.N. Haining, G.J. Freeman, and A.H. Sharpe. 2017. PD-L1 on tumor cells is sufficient for immune evasion in immunogenic tumors and inhibits CD8 T cell cytotoxicity. *J. Exp. Med*. 214:895–904. https://doi.org/10.1084/jem.20160801

Kamphorst, A.O., A. Wieland, T. Nasti, S. Yang, R. Zhang, D.L. Barber, B.T. Konieczny, C.Z. Daugherty, L. Koenig, K. Yu, et al. 2017. Rescue of exhausted CD8 T cells by PD-1-targeted therapies is CD28-dependent. *Science*. 355:1423–1427. https://doi.org/10.1126/science.aaf0683

Keir, M.E., S.C. Liang, I. Guleria, Y.E. Latchman, A. Qipo, L.A. Albacker, M. Koulmanda, G.J. Freeman, M.H. Sayegh, and A.H. Sharpe. 2006. Tissue expression of PD-L1 mediates peripheral T cell tolerance. *J. Exp. Med*. 203:883–895. https://doi.org/10.1084/jem.20051776

Kishton, R.J., C.E. Barnes, A.G. Nichols, S. Cohen, V.A. Gerriets, P.J. Siska, A.N. Macintyre, P. Goraksha-Hicks, A.A. de Cubas, T. Liu, et al. 2016. AMPK Is Essential to Balance Glycolysis and Mitochondrial Metabolism to Control T-ALL Cell Stress and Survival. *Cell Metab*. 23:649–662. https://doi.org/10.1016/j.cmet.2016.03.008

Kroner, A., N. Schwab, C.W. Ip, S. Ortler, K. Göbel, K.A. Nave, M. Mäurer, R. Martini, and H. Wiendl. 2009. Accelerated course of experimental autoimmune encephalomyelitis in PD-1-deficient central nervous system myelin mutants. *Am. J. Pathol*. 174:2290–2299. https://doi.org/10.2353/ajpath.2009.081012

Latchman, Y.E., S.C. Liang, Y. Wu, T. Chernova, R.A. Sobel, M. Klemm, V.K. Kuchroo, G.J. Freeman, and A.H. Sharpe. 2004. PD-L1-deficient mice show that PD-L1 on T cells, antigen-presenting cells, and host tissues negatively regulates T cells. *Proc. Natl. Acad. Sci. USA*. 101:10691–10696. https://doi.org/10.1073/pnas.0307252101

Liang, S.C., Y.E. Latchman, J.E. Buhlmann, M.F. Tomczak, B.H. Horwitz, G.J. Freeman, and A.H. Sharpe. 2003. Regulation of PD-1, PD-L1, and PD-L2 expression during normal and autoimmune responses. *Eur. J. Immunol*. 33:2706–2716. https://doi.org/10.1002/eji.200324228

MacIver, N.J., R.D. Michalek, and J.C. Rathmell. 2013. Metabolic regulation of T lymphocytes. *Annu. Rev. Immunol*. 31:259–283. https://doi.org/10.1146/annurev-immunol-032712-095956

Mikami, N., and S. Sakaguchi. 2014. CD28 signals the differential control of regulatory T cells and effector T cells. *Eur. J. Immunol*. 44:955–957. https://doi.org/10.1002/eji.201444513

Miyao, T., S. Floess, R. Setoguchi, H. Luche, H.J. Fehling, H. Waldmann, J. Huehn, and S. Hori. 2012. Plasticity of Foxp3(+) T cells reflects promiscuous Foxp3 expression in conventional T cells but not reprogramming of regulatory T cells. *Immunity*. 36:262–275. https://doi.org/10.1016/j.immuni.2011.12.012

Okazaki, T., S. Chikuma, Y. Iwai, S. Fagarasan, and T. Honjo. 2013. A rheostat for immune responses: the unique properties of PD-1 and their advantages for clinical application. *Nat. Immunol*. 14:1212–1218. https://doi.org/10.1038/ni.2762

Pardoll, D.M. 2012. Immunology beats cancer: a blueprint for successful translation. *Nat. Immunol*. 13:1129–1132. https://doi.org/10.1038/ni.2392

Parry, R.V., J.M. Chemnitz, K.A. Frauwirth, A.R. Lanfranco, I. Braunstein, S.V. Kobayashi, P.S. Linsley, C.B. Thompson, and J.L. Riley. 2005. CTLA-4 and PD-1 receptors inhibit T-cell activation by distinct mechanisms. *Mol. Cell. Biol*. 25:9543–9553. https://doi.org/10.1128/MCB.25.21.9543-9553.2005

Patel, S.P., and R. Kurzrock. 2015. PD-L1 Expression as a Predictive Biomarker in Cancer Immunotherapy. *Mol. Cancer Ther*. 14:847–856. https://doi.org/10.1158/1535-7163.MCT-14-0983

Paterson, A.M., K.E. Brown, M.E. Keir, V.K. Vanguri, L.V. Riella, A. Chandraker, M.H. Sayegh, B.R. Blazar, G.J. Freeman, and A.H. Sharpe. 2011. The programmed death-1 ligand 1:B7-1 pathway restrains diabetogenic effector T cells in vivo. *J. Immunol*. 187:1097–1105. https://doi.org/10.4049/jimmunol.1003496

Patsoukis, N., J. Brown, V. Petkova, F. Liu, L. Li, and V.A. Boussiotis. 2012. Selective effects of PD-1 on Akt and Ras pathways regulate molecular

components of the cell cycle and inhibit T cell proliferation. *Sci. Signal.* 5:ra46. https://doi.org/10.1126/scisignal.2002796

Patsoukis, N., L. Li, D. Sari, V. Petkova, and V.A. Boussiotis. 2013. PD-1 increases PTEN phosphatase activity while decreasing PTEN protein stability by inhibiting casein kinase 2. *Mol. Cell. Biol.* 33:3091–3098. https://doi.org/10.1128/MCB.00319-13

Patsoukis, N., K. Bardhan, P. Chatterjee, D. Sari, B. Liu, L.N. Bell, E.D. Karoly, G.J. Freeman, V. Petkova, P. Seth, et al. 2015. PD-1 alters T-cell metabolic reprogramming by inhibiting glycolysis and promoting lipolysis and fatty acid oxidation. *Nat. Commun.* 6:6692. https://doi.org/10.1038/ncomms7692

Pauken, K.E., and E.J. Wherry. 2015. Overcoming T cell exhaustion in infection and cancer. *Trends Immunol.* 36:265–276. https://doi.org/10.1016/j.it.2015.02.008

Price, N.L., A.P. Gomes, A.J. Ling, F.V. Duarte, A. Martin-Montalvo, B.J. North, B. Agarwal, L. Ye, G. Ramadori, J.S. Teodoro, et al. 2012. SIRT1 is required for AMPK activation and the beneficial effects of resveratrol on mitochondrial function. *Cell Metab.* 15:675–690. https://doi.org/10.1016/j.cmet.2012.04.003

Reynoso, E.D., K.G. Elpek, L. Francisco, R. Bronson, A. Bellemare-Pelletier, A.H. Sharpe, G.J. Freeman, and S.J. Turley. 2009. Intestinal tolerance is converted to autoimmune enteritis upon PD-1 ligand blockade. *J. Immunol.* 182:2102–2112. https://doi.org/10.4049/jimmunol.0802769

Riley, J.L. 2009. PD-1 signaling in primary T cells. *Immunol. Rev.* 229:114–125. https://doi.org/10.1111/j.1600-065X.2009.00767.x

Rosenblum, M.D., I.K. Gratz, J.S. Paw, and A.K. Abbas. 2012. Treating human autoimmunity: current practice and future prospects. *Sci. Transl. Med.* 4. 125sr1. https://doi.org/10.1126/scitranslmed.3003504

Rubtsov, Y.P., J.P. Rasmussen, E.Y. Chi, J. Fontenot, L. Castelli, X. Ye, P. Treuting, L. Siewe, A. Roers, W.R. Henderson, Jr., et al. 2008. Regulatory T cell-derived interleukin-10 limits inflammation at environmental interfaces. *Immunity.* 28:546–558. https://doi.org/10.1016/j.immuni.2008.02.017

Sage, P.T., N. Ron-Harel, V.R. Juneja, D.R. Sen, S. Maleri, W. Sungnak, V.K. Kuchroo, W.N. Haining, N. Chevrier, M. Haigis, et al. 2016. Suppression by T_{FR} cells leads to durable and selective inhibition of B cell effector function. *Nat. Immunol.* 17:1436–1446. https://doi.org/10.1038/ni.3578

Salama, A.D., T. Chitnis, J. Imitola, M.J. Ansari, H. Akiba, F. Tushima, M. Azuma, H. Yagita, M.H. Sayegh, and S.J. Khoury. 2003. Critical role of the programmed death-1 (PD-1) pathway in regulation of experimental autoimmune encephalomyelitis. *J. Exp. Med.* 198:71–78. https://doi.org/10.1084/jem.20022119

Sauer, S., L. Bruno, A. Hertweck, D. Finlay, M. Leleu, M. Spivakov, Z.A. Knight, B.S. Cobb, D. Cantrell, E. O'Connor, et al. 2008. T cell receptor signaling controls Foxp3 expression via PI3K, Akt, and mTOR. *Proc. Natl. Acad. Sci. USA.* 105:7797–7802. https://doi.org/10.1073/pnas.0800928105

Scandiuzzi, L., K. Ghosh, K.A. Hofmeyer, Y.M. Abadi, E. Lázár-Molnár, E.Y. Lin, Q. Liu, H. Jeon, S.C. Almo, L. Chen, et al. 2014. Tissue-expressed B7-H1 critically controls intestinal inflammation. *Cell Rep.* 6:625–632. https://doi.org/10.1016/j.celrep.2014.01.020

Schreiner, B., M. Mitsdoerffer, B.C. Kieseier, L. Chen, H.P. Hartung, M. Weller, and H. Wiendl. 2004. Interferon-beta enhances monocyte and dendritic cell expression of B7-H1 (PD-L1), a strong inhibitor of autologous T-cell activation: relevance for the immune modulatory effect in multiple sclerosis. *J. Neuroimmunol.* 155:172–182. https://doi.org/10.1016/j.jneuroim.2004.06.013

Selby, M.J., J.J. Engelhardt, M. Quigley, K.A. Henning, T. Chen, M. Srinivasan, and A.J. Korman. 2013. Anti-CTLA-4 antibodies of IgG2a isotype enhance antitumor activity through reduction of intratumoral regulatory T cells. *Cancer Immunol. Res.* 1:32–42. https://doi.org/10.1158/2326-6066.CIR-13-0013

Sharpe, A.H., and K.E. Pauken. 2018. The diverse functions of the PD1 inhibitory pathway. *Nat. Rev. Immunol.* 18:153–167. https://doi.org/10.1038/nri.2017.108

Sheppard, K.A., L.J. Fitz, J.M. Lee, C. Benander, J.A. George, J. Wooters, Y. Qiu, J.M. Jussif, L.L. Carter, C.R. Wood, et al. 2004. PD-1 inhibits T-cell receptor induced phosphorylation of the ZAP70/CD3zeta signalosome and downstream signaling to PKCtheta. *FEBS Lett.* 574:37–41. https://doi.org/10.1016/j.febslet.2004.07.083

Simpson, T.R., F. Li, W. Montalvo-Ortiz, M.A. Sepulveda, K. Bergerhoff, F. Arce, C. Roddie, J.Y. Henry, H. Yagita, J.D. Wolchok, et al. 2013. Fc-dependent depletion of tumor-infiltrating regulatory T cells co-defines the efficacy of anti-CTLA-4 therapy against melanoma. *J. Exp. Med.* 210:1695–1710. https://doi.org/10.1084/jem.20130579

Smigiel, K.S., S. Srivastava, J.M. Stolley, and D.J. Campbell. 2014. Regulatory T-cell homeostasis: steady-state maintenance and modulation during inflammation. *Immunol. Rev.* 259:40–59. https://doi.org/10.1111/imr.12170

Topalian, S.L., M. Sznol, D.F. McDermott, H.M. Kluger, R.D. Carvajal, W.H. Sharfman, J.R. Brahmer, D.P. Lawrence, M.B. Atkins, J.D. Powderly, et al. 2014. Survival, durable tumor remission, and long-term safety in patients with advanced melanoma receiving nivolumab. *J. Clin. Oncol.* 32:1020–1030. https://doi.org/10.1200/JCO.2013.53.0105

Vignali, D.A., L.W. Collison, and C.J. Workman. 2008. How regulatory T cells work. *Nat. Rev. Immunol.* 8:523–532. https://doi.org/10.1038/nri2343

Wang, J., T. Yoshida, F. Nakaki, H. Hiai, T. Okazaki, and T. Honjo. 2005. Establishment of NOD-Pdcd1-/- mice as an efficient animal model of type I diabetes. *Proc. Natl. Acad. Sci. USA.* 102:11823–11828. https://doi.org/10.1073/pnas.0505497102

Wang, L., K. Pino-Lagos, V.C. de Vries, I. Guleria, M.H. Sayegh, and R.J. Noelle. 2008. Programmed death 1 ligand signaling regulates the generation of adaptive Foxp3+CD4+ regulatory T cells. *Proc. Natl. Acad. Sci. USA.* 105:9331–9336. https://doi.org/10.1073/pnas.0710441105

Wang, C., B. Dehghani, Y. Li, L.J. Kaler, A.A. Vandenbark, and H. Offner. 2009. Oestrogen modulates experimental autoimmune encephalomyelitis and interleukin-17 production via programmed death 1. *Immunology.* 126:329–335. https://doi.org/10.1111/j.1365-2567.2008.03051.x

Wing, K., Y. Onishi, P. Prieto-Martin, T. Yamaguchi, M. Miyara, Z. Fehervari, T. Nomura, and S. Sakaguchi. 2008. CTLA-4 control over Foxp3+ regulatory T cell function. *Science.* 322:271–275. https://doi.org/10.1126/science.1160062

Wolchok, J.D., H. Kluger, M.K. Callahan, M.A. Postow, N.A. Rizvi, A.M. Lesokhin, N.H. Segal, C.E. Ariyan, R.A. Gordon, K. Reed, et al. 2013. Nivolumab plus ipilimumab in advanced melanoma. *N. Engl. J. Med.* 369:122–133. https://doi.org/10.1056/NEJMoa1302369

Yan, D., J. Farache, M. Mingueneau, D. Mathis, and C. Benoist. 2015. Imbalanced signal transduction in regulatory T cells expressing the transcription factor FoxP3. *Proc. Natl. Acad. Sci. USA.* 112:14942–14947. https://doi.org/10.1073/pnas.1520393112

Yearley, J.H., C. Gibson, N. Yu, C. Moon, E. Murphy, J. Juco, J. Lunceford, J. Cheng, L.Q.M. Chow, T.Y. Seiwert, et al. 2017. PD-L2 Expression in Human Tumors: Relevance to Anti-PD-1 Therapy in Cancer. *Clin. Cancer Res.* 23:3158–3167. https://doi.org/10.1158/1078-0432.CCR-16-1761

Zhang, B., S. Chikuma, S. Hori, S. Fagarasan, and T. Honjo. 2016. Nonoverlapping roles of PD-1 and FoxP3 in maintaining immune tolerance in a novel autoimmune pancreatitis mouse model. *Proc. Natl. Acad. Sci. USA.* 113:8490–8495. https://doi.org/10.1073/pnas.1608873113

Zhou, X., L.T. Jeker, B.T. Fife, S. Zhu, M.S. Anderson, M.T. McManus, and J.A. Bluestone. 2008. Selective miRNA disruption in T reg cells leads to uncontrolled autoimmunity. *J. Exp. Med.* 205:1983–1991. https://doi.org/10.1084/jem.20080707

Supplemental material

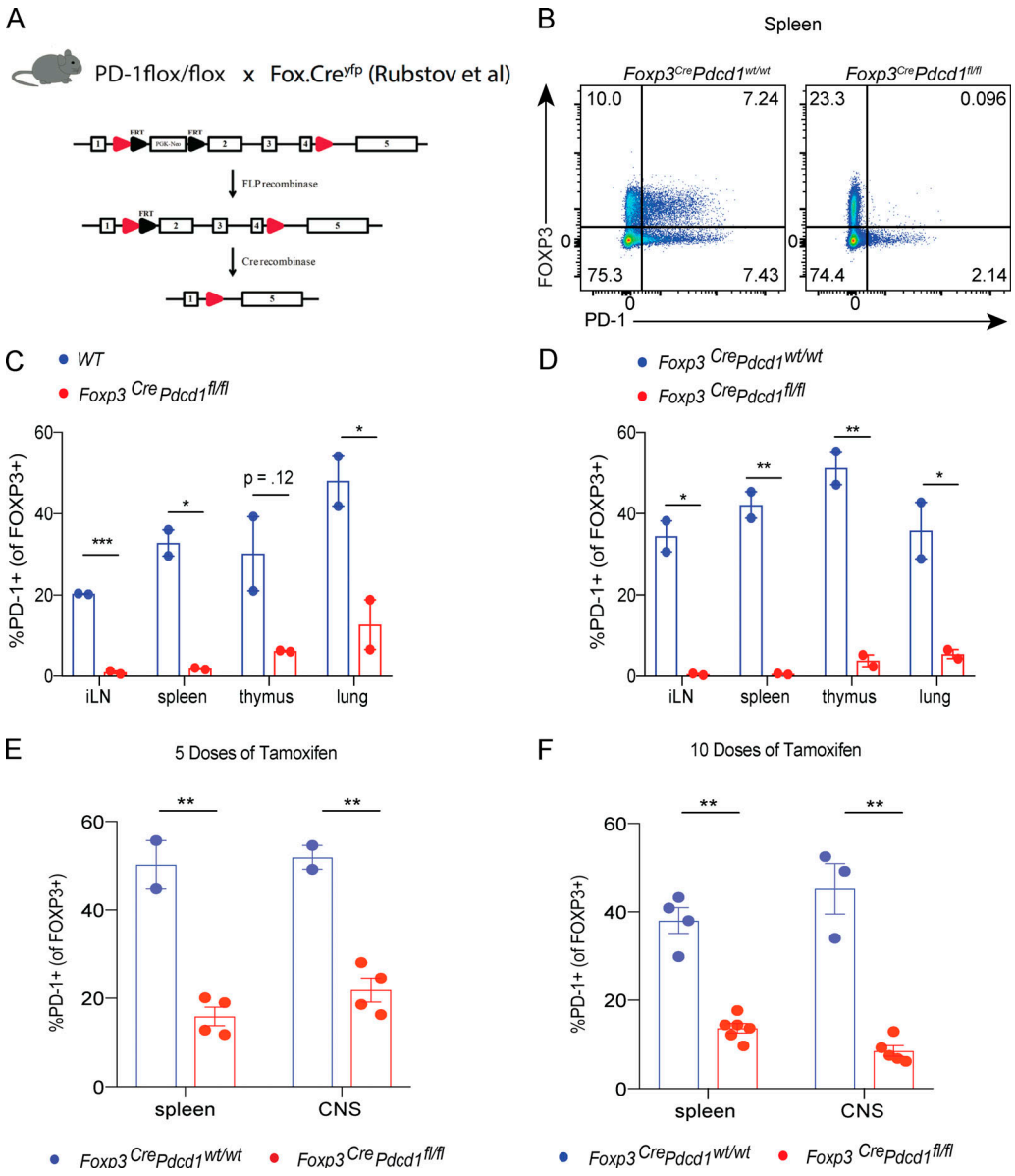

Figure S1. **Generation and characterization of mice selectively lacking PD-1 on T reg cells. (A)** Schematic showing generation of T reg cell–specific PD-1 conditional knockout mice, referred to as *Foxp3*^{Cre} *Pdcd1*$^{fl/fl}$ mice. **(B)** Spleens from *Foxp3*^{Cre} *Pdcd1*$^{wt/wt}$ or *Foxp3*^{Cre} *Pdcd1*$^{fl/fl}$ littermate mice were analyzed for PD-1 expression. Plots are gated on CD4^{+} cells (C–G). **(C)** Quantification of PD-1 expression on T reg cells from inguinal LN (iLN), spleen, thymus, and lung of naive *Foxp3*^{Cre} *Pdcd-1*$^{fl/fl}$ (n = 2) and WT mice (n = 2) at 4–5 wk of age. **(D)** Quantification of PD-1 expression on T reg cells from inguinal LN (iLN), spleen, thymus and lung of naive *Foxp3*^{Cre} *Pdcd1*$^{fl/fl}$ (n = 2) and *Foxp3*^{Cre} *Pdcd1*$^{wt/wt}$ (n = 2) littermate mice at 8 wk of age. **(E and F)** Quantification of PD-1 expression on T reg cells from spleen and CNS of *iFoxp3*^{Cre} *Pdcd1*$^{fl/fl}$ and *iFoxp3*^{Cre} *Pdcd1*$^{wt/wt}$ littermate mice given 5 doses of tamoxifen (*iFoxp3*^{Cre} *Pdcd1*$^{fl/fl}$ n = 4 and *iFoxp3*^{Cre} *Pdcd1*$^{wt/wt}$ n = 2; E) or 10 doses of tamoxifen (*iFoxp3*^{Cre} *Pdcd1*$^{fl/fl}$ n = 6 and *iFoxp3*^{Cre} *Pdcd1*$^{wt/wt}$ n = 3–4; F) and then immunized to induce EAE with $MOG_{35–55}$/CFA. PD-1 expression was analyzed at day 12 (E) and day 13 (F) after immunization. B is representative of three independent experiments; C and D have been completed once. E and F are representative of at least two independent experiments. Data are represented means ± SEM. Significance was assessed using Student's t test. *, P < 0.05; **, P < 0.01; ***, P < 0.005.

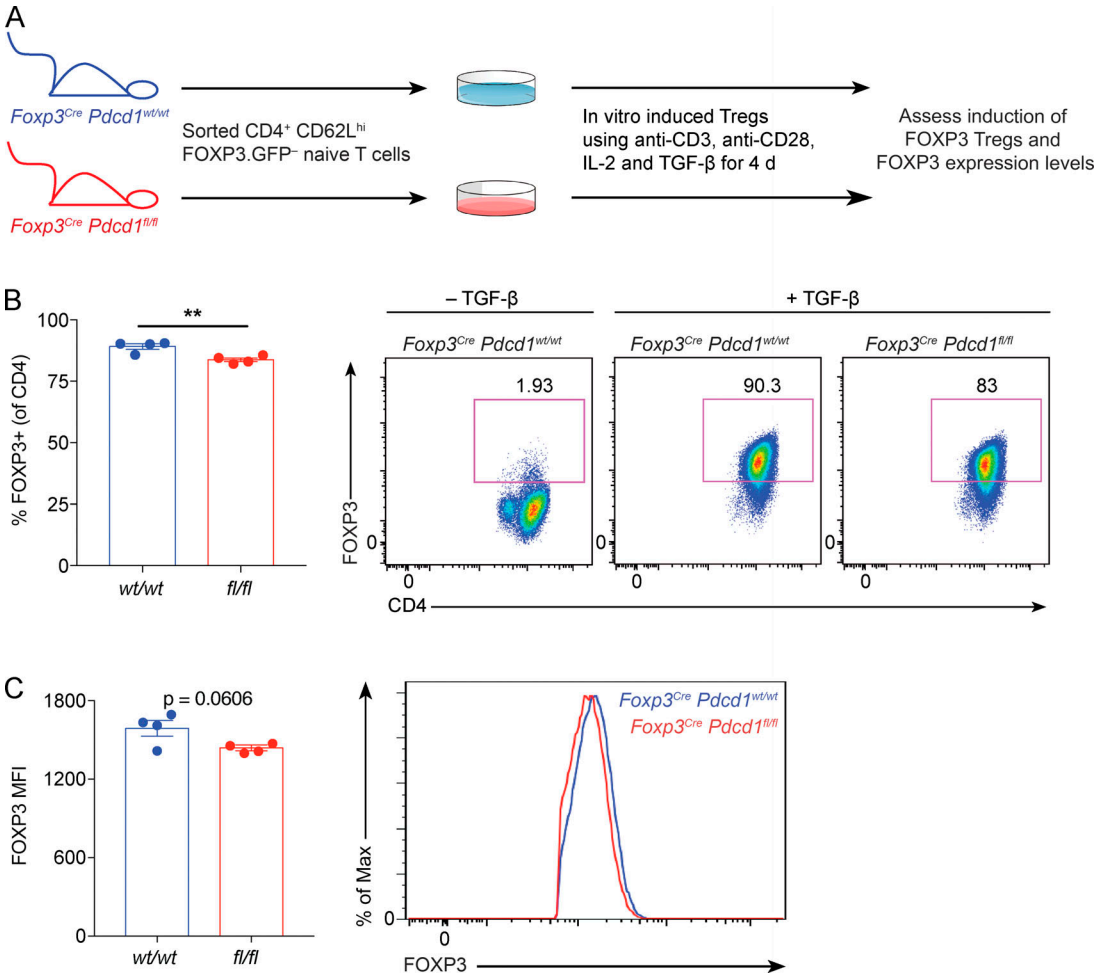

Figure S2. **Induction of iT reg cells from *FoxP3*^{Cre} *Pdcd1*$^{fl/fl}$ mice. (A)** Experimental design of in vitro T reg cell differentiation assay using naive CD4$^+$ T cells from *Foxp3*^{Cre} *Pdcd1*$^{fl/fl}$ (red circles, *n* = 4) or littermate control *Foxp3*^{Cre} *Pdcd1*$^{wt/wt}$ (blue circles, *n* = 4) mice. **(B)** Percentages of FOXP3-expressing T reg cells induced after 4 d of in vitro differentiation. Quantification of percentage of FOXP3-expressing CD4$^+$ T cells (left) and representative flow plots of percentages of FOXP3-expressing CD4$^+$ T cells (right). **(C)** Summary of quantification of expression level of FOXP3 (left) and representative histogram of FOXP3 expression levels (right) in the in vitro induced FOXP3-expressing T reg cells from *Foxp3*^{Cre} *Pdcd1*$^{wt/wt}$ (blue circles, *n* = 4)) or *Foxp3*^{Cre} *Pdcd1*$^{fl/fl}$ (red circles, *n* = 4) mice. MFI, mean fluorescence intensity. Significance was assessed using a Student's *t* test. **, P < 0.01.

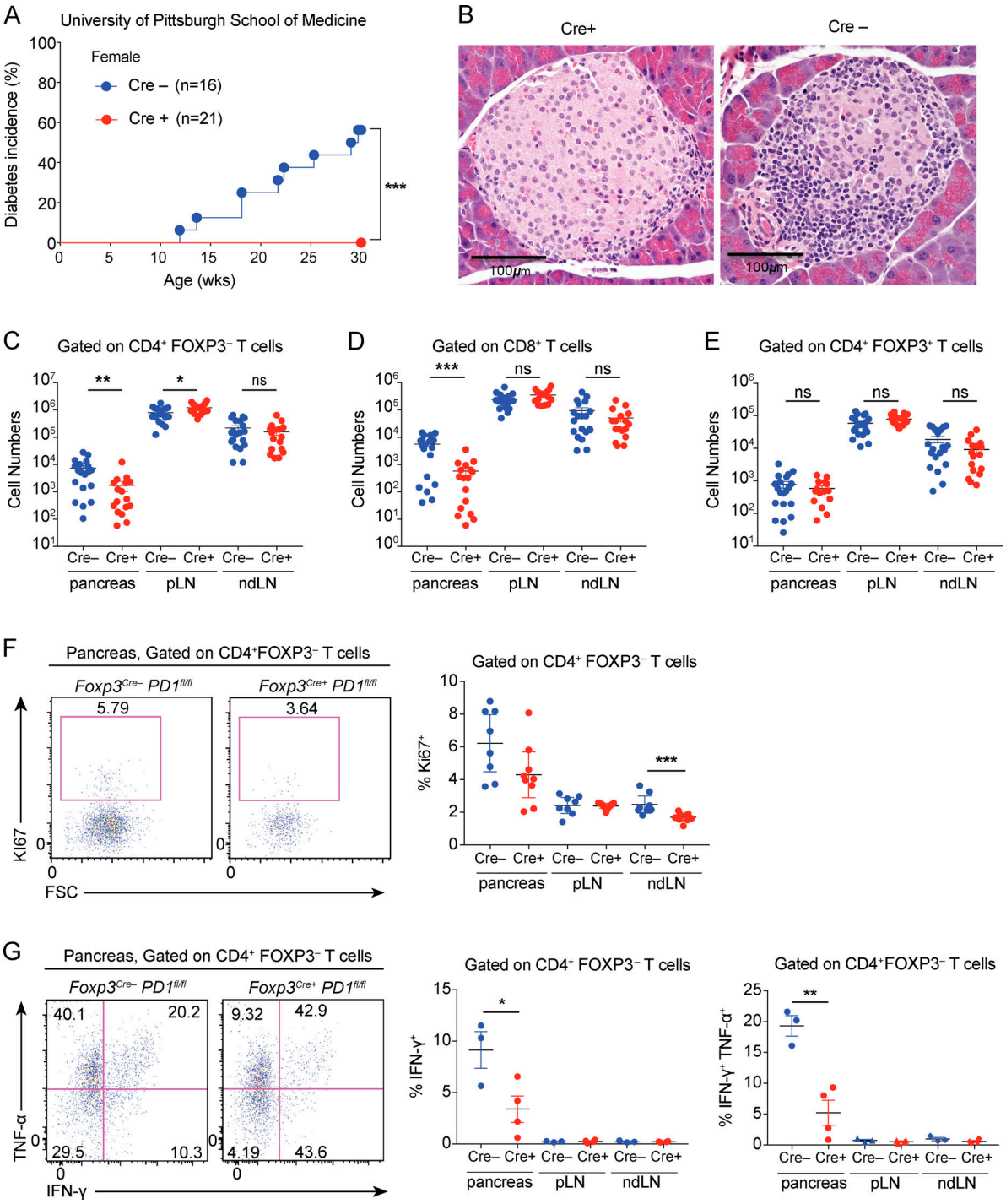

Figure S3. **Immune characterization of *NOD.Foxp3^{Cre} Pdcd1$^{fl/fl}$* mice. (A)** Diabetes onset and incidence were monitored in cohoused *NOD.Foxp3^{Cre+} Pdcd1$^{fl/fl}$* (red, *n* = 21) and *NOD.Foxp3$^{Cre–}$ Pdcd1$^{fl/fl}$* (blue, *n* = 16) females in an animal facility at the University of Pittsburgh School of Medicine to up to 30 wk of age. **(B)** Representative H&E staining of an islet from *NOD.Foxp3^{Cre+} Pdcd1$^{fl/fl}$* and *NOD.Foxp3$^{Cre–}$ Pdcd1$^{fl/fl}$* littermates at 14 wk of age. **(C–E)** Numbers of CD4$^+$ FOXP3$^–$ Teff cells (C), CD8$^+$ T cells (D), and CD4$^+$ FOXP3$^+$ T reg cells (E) from the pancreas, pLN, and ndLN from Cre+ (red circles, *n* = 17) and Cre– (blue circles, *n* = 20) littermate controls at 14 wk of age. **(F)** Representative flow cytometry plots from the pancreas (left panel) and quantified percentages (right panel) of Ki67-expressing CD4$^+$ FOXP3$^–$ Teff cells from the pancreas, pLN, and ndLN of prediabetic *NOD.Foxp3$^{Cre–}$ Pdcd1$^{fl/fl}$* (Cre–, blue circles, *n* = 8) and *NOD.Foxp3^{Cre+} Pdcd1$^{fl/fl}$* (Cre+, red circles, *n* = 9) mice at 14 wk of age. **(G)** CD4$^+$ FOXP3$^–$ Teff cells from the pancreas, pLN, and ndLN of prediabetic *NOD.Foxp3$^{Cre–}$ Pdcd1$^{fl/fl}$* (Cre–, blue circles, *n* = 3) and *NOD.Foxp3^{Cre+} Pdcd1$^{fl/fl}$* (Cre+, red circles, *n* = 4) mice were analyzed for IFN-γ and TNF-α production by intracellular staining at 14 wk of age. Representative plots (left panel) from the pancreas and percentages (right panel) of IFN-γ and TNF-α production are shown. Data are pooled from four independent experiments (C–E) or representative of two independent experiments (F and G). A log-rank (Mantel–Cox) test (A), Mann–Whitney non-parametric test (C–E), or Student's *t* test (F and G) was used. Data are shown as means ± SEM. *, P < 0.05; **, P < 0.01; ***, P < 0.005. ns, not significant.

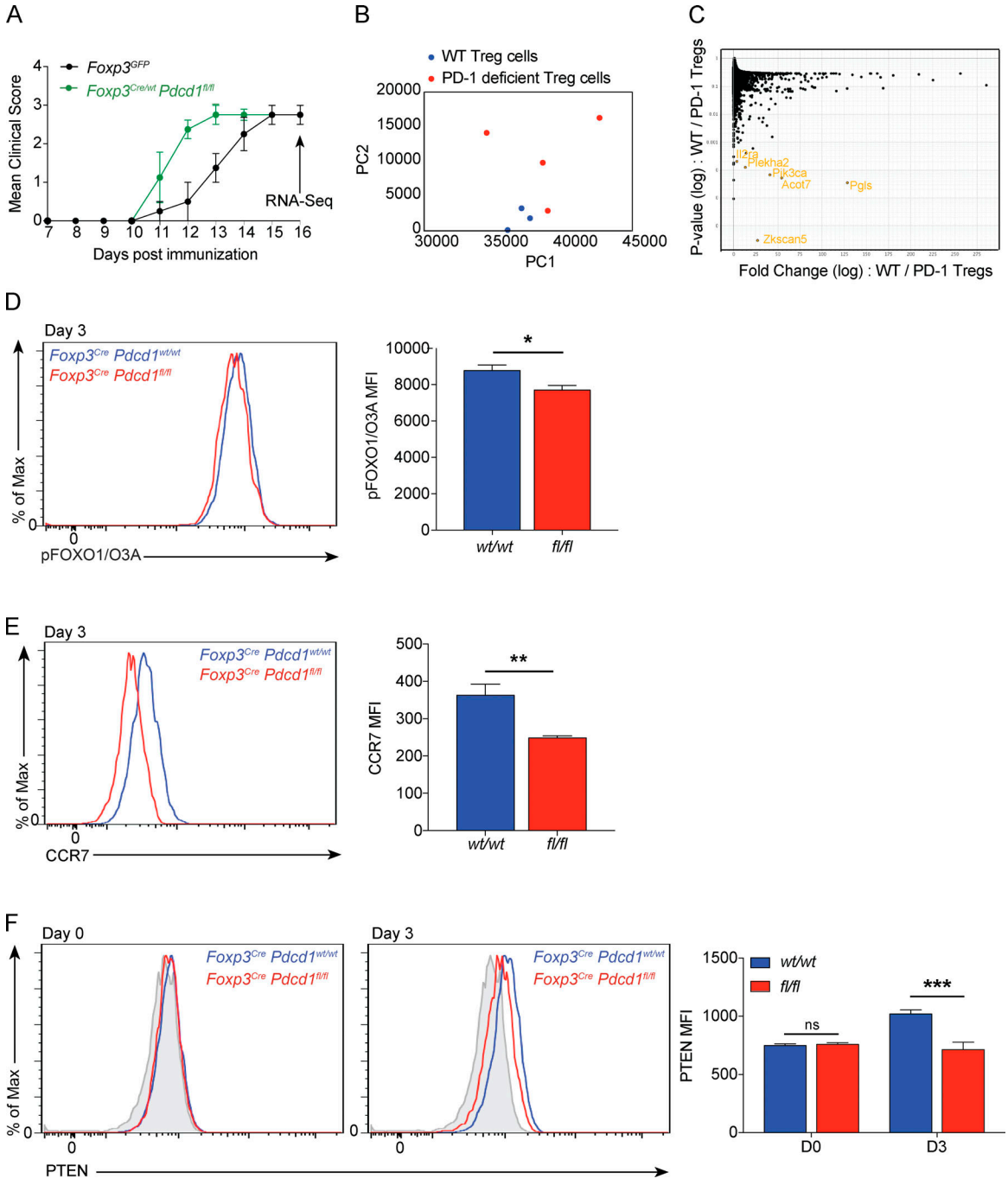

Figure S4. **Validation of transcriptional analysis of WT and PD-1–deficient T reg cells. (A)** EAE disease scores of mice used for transcriptional analysis. **(B)** Principal-component (PC) analysis plot of individual samples for RNA-seq analysis. **(C)** Volcano plots showing differential gene expression in WT versus PD-1–deficient T reg cell populations. **(D)** Representative histogram of expression levels of pFox01/03A (left) with summary of quantification of pFOXO1/O3A (right) in WT (blue, *n* = 4) and PD-1–deficient T reg cells (red, *n* = 4) during an in vitro T reg cell–mediated suppression assay at indicated time points. MFI, mean fluorescence intensity. **(E)** Representative histogram of expression levels of CCR7 (left) with summary of quantification of CCR7 levels (right) in WT (blue, *n* = 4) and PD-1–deficient T reg cells (red, *n* = 4) during an in vitro T reg cell–mediated suppression assay during indicated time points. **(F)** Representative histogram of expression levels of PTEN (left) with summary of quantification of PTEN levels (right) in WT (blue, *n* = 4) and PD-1–deficient T reg cells (red, *n* = 4) during an in vitro T reg cell–mediated suppression assay at indicated time points. Data are shown as means ± SEM. RNA-seq was conducted once but with biological replicates (*Foxp3*^{GFP} control, *n* = 3 and *Foxp3*$^{Cre.YFP/wt}$ *Pdcd1*$^{fl/fl}$, *n* = 4). Phospho-flow cytometry analysis and T reg cell–mediated in vitro suppression assay data are representative of three independent experiments. Significance was assessed using a Student's *t* test. *, P < 0.05; **, P < 0.01; ***, P < 0.005.

Table S1 is provided online as a separate Excel file and shows a summary of gene set enrichment analyses comparing WT and PD-1–deficient T reg cells.